Title

Comparison of Ciliary Targeting of Two Rhodopsin-Like GPCRs: Role of C-Terminal Localization Sequences in Relation to Cilium Type

Journal

Journal of Neuroscience, 41(36)

ISSN

0270-6474

Authors

Chadha, Abhishek
Paniagua, Antonio E
Williams, David S

Publication Date

2021-09-08

DOI

10.1523/jneurosci.0357-21.2021

Peer reviewed

Cellular/Molecular

Comparison of Ciliary Targeting of Two Rhodopsin-Like GPCRs: Role of C-Terminal Localization Sequences in Relation to Cilium Type

Abhishek Chadha,[1,2] **Antonio E. Paniagua,**[1,2] **and David S. Williams**[1,2,3,4]

[1]Departments of Ophthalmology and Neurobiology, [2]Stein Eye Institute, [3]Molecular Biology Institute, and [4]David Geffen School of Medicine, Brain Research Institute, University of California, Los Angeles, Los Angeles, California 90095

Primary cilia exhibit a distinct complement of proteins, including G-protein-coupled receptors (GPCRs) that mediate sensory and developmental signals. The localization of GPCRs to the ciliary membrane involves ciliary localization sequences (CLSs), but it is not known how CLSs might relate to cilium type. Here, we studied the localization of two rhodopsin (RHO)-like GPCRs, somatostatin receptor (SSTR3) and RHO, in three types of cilia, from inner medullary collecting duct (IMCD3) cells, hTERT-RPE1 cells (possessing pocket cilia), and rod photoreceptors (whose cilia grow into elaborate phototransductive outer segments). SSTR3 was localized specifically to all three types of cilia, whereas RHO showed more selectivity for the photoreceptor cilium. Focusing on C-terminal CLSs, we characterized a novel CLS in the SSTR3 C terminus, which was required for the robust ciliary localization of SSTR3. Replacing the C terminus of RHO with this SSTR3 CLS-enhanced ciliary localization, compared with full-length RHO in IMCD3 and hTERT-RPE1 cells. Addition of the SSTR3 CLS to the single transmembrane protein CD8A enabled ciliary localization. In hTERT-RPE1 cells, a partial SSTR3 CLS added to CD8A effected specific localization to the periciliary (pocket) membrane, demonstrating C-terminal localization sequence targeting to this domain. Using retinas from mice, including both sexes, we show that deletion of the C terminus of RHO reduced the rod outer segment localization and that addition of the SSTR3 C-terminal CLS to the truncated RHO partly rescued this mislocalization. Overall, the study details elements of the different C termini of SSTR3 and RHO that are major effectors in determining specificity of cilium (or pericilium) localization among different types of cilia.

Key words: **cilium; localization sequence; protein targeting; rhodopsin; SSTR3**

Significance Statement

The localization of G-protein-coupled receptors to primary cilia is key to many types of signal transduction. After characterizing a novel C-terminal CLS in SSTR3, we investigated how SSTR3 and RHO localization to the cilium relates to C-terminal CLSs and to cilium type. We found that the SSTR3 C-terminal CLS was effective in three different types of cilia, but the RHO C terminus showed a clear localization preference for the highly elaborate photoreceptor cilium. When added to CD8A, part of the SSTR3 CLS promoted specific periciliary membrane localization in hTERT-RPE1 cells, demonstrating an effective CLS for this domain. Thus, we demonstrate that elements of the C termini of SSTR3 and RHO determine different localization patterns among different types of cilia.

Introduction

Primary cilia are small microtubule-based structures involved in the detection of extracellular signals. The ciliary membrane exhibits a composition that is distinct from that of the plasma membrane, including an enrichment of sensory receptors (Corbit et al., 2005; Hu et al., 2010; Nemet et al., 2015; Garcia et al., 2018). Localization to the ciliary membrane is key for the function of many G-protein-coupled receptors (GPCRs). For example, the rhodopsin (RHO)-like somatostatin receptor 3 (SSTR3) is localized to the neuronal cilia of the CNS (Guadiana et al., 2016), where it functions in novel object recognition in mice, possibly via ciliary cAMP signaling (Einstein et al., 2010). The localization of Smoothened to the cilium is dynamically regulated by the ciliary binding of the Hh ligand to Patched1 and leads to the activation of Gli transcription factors (Wong and Reiter, 2008).

Received Feb. 10, 2021; revised May 20, 2021; accepted June 16, 2021.

Author contributions: A.C., A.E.P., and D.S.W. designed research; A.C. and A.E.P. performed research; A.C. and D.S.W. analyzed data; A.C. and D.S.W. wrote the paper.

This work was supported by National Institutes of Health Grants F32EY026318 (A.C.), R01EY013408 and R01EY027442 and P30EY00331 (D.S.W.). We thank Barry Burgess and Carrie Louie for technical assistance.

The authors declare no competing financial interests.

Correspondence should be addressed to David S. Williams at dswilliams@ucla.edu.

https://doi.org/10.1523/JNEUROSCI.0357-21.2021

The most extreme example of GPCR ciliary localization occurs in vertebrate photoreceptor cells. The ciliary plasma membrane of photoreceptors is extensively amplified into disk membranes (Sjostrand, 1953; Steinberg et al., 1980; Burgoyne et al., 2015; Ding et al., 2015; Volland et al., 2015), which contain vast amounts of RHO (Papermaster and Dreyer, 1974; Nickell et al., 2007). The formation and continual renewal of these disk membranes requires the movement of large amounts of RHO into the cilium and along the ciliary plasma membrane to the site of disk morphogenesis: an average of 72 RHO molecules per second in a mouse rod (Williams, 2002), and 1000 molecules per second in the larger frog rod (Papermaster et al., 1985). Gene mutations resulting in defects in RHO localization to the outer segment underlie retinal degenerations in animal models and humans; for example, mutations in *Myo7a*, *Tulp1, Bbs2, RHO* (P23H), and TUB (Dryja et al., 1990; Liu et al., 1999; Nishimura et al., 2004; Lopes et al., 2010; Grossman et al., 2011; Borman et al., 2014).

Our understanding of how GPCRs are localized to cilia has focused on motifs within the intracellular domains of GPCRs. Such ciliary localization sequences (CLS) have been identified in the C terminus and the third intracellular loop of GPCRs. In RHO a motif consisting of the last four amino acids of the C terminus, VxPx, has been identified as a CLS, required for enrichment of RHO in the outer segment (Li et al., 1996; Tam et al., 2000; Concepcion and Chen, 2010; Lodowski et al., 2013; Pearring et al., 2013). By contrast, SSTR3 has been reported to use dual Ax(S/A)xQ motifs in its third intracellular loop (IC3) for ciliary localization (Berbari et al., 2008a; Geneva et al., 2017).

Here, we have considered the specificity of CLSs. We have addressed whether the CLSs within different GPCRs might show different preferences for different types of cilia. Our results show that SSTR3 undergoes highly specific localization to a broad range of types of cilia, whereas the localization of RHO, while highly specific to the photoreceptor cilium [outer segment (OS)], is targeted less specifically to less elaborate primary cilia. To understand these localization behaviors better, we furthered CLS characterization in SSTR3, by defining a novel CLS in the C terminus, and we compared and contrasted the localization function of this C-terminal CLS with that of the RHO C terminus in different types of cilia.

Materials and Methods

Cell culture. We obtained previously validated cell lines from the American Type Culture Collection (hTERT-RPE1, CRL-4000; IMCD3, CRL-2123). IMCD3 and hTERT-RPE1 cells, which had been passaged 15–30 times, were maintained in DMEM-F12 with 10% FBS and 1% penicillin and streptomycin. IMCD3 cells were grown on glass coverslips, and RPE1 cells were grown on Ibidi #1 chambered coverslips. For all IMCD3 experiments and most hTERT-RPE1 experiments, expression was achieved by transient transfection. For some hTERT-RPE1 experiments, a stable lentivirus transduced cell line, expressing RHO-EGFP-C8 and SSTR3-670, was used. We confirmed that the localization of RHO-EGFP-C8 and SSTR3-670 was not different between transiently transfected and stably transduced cells.

Cells were transfected with Lipofectamine 3000 (Thermo Fisher Scientific) for IMCD3 cells or jetPRIME (Polyplus Transfection) for hTERT-RPE1 cells. They were transfected for 16–24 h and serum starved for 24–48 h before imaging. Ibidi chambered coverslips containing RPE1 cells were imaged directly; coverslips with IMCD3 cells were inverted and placed on 35 mm Ibidi chambered coverslips to promote cilium flattening. Liquid was wicked away, and the edges of the coverslips were coated with vacuum grease to prevent the cells from drying out during imaging.

Avitag-labeled constructs were expressed in cells that were grown in 10 μM biotin (Avidity). Cells were cotransfected with pDisplay-BirA-ER, which biotinylates avitag-labeled proteins in the endoplasmic reticulum (Howarth et al., 2005). We labeled cells with 20 μg/ml extracellular streptavidin-Alexa Fluor 488 (Thermo Fisher Scientific) for 10 min at room temperature, then washed them three times with DPBS containing 0.9 mM Ca^{2+} and 0.5 mM Mg^{2+} before imaging.

For clustered regularly interspaced short palindromic repeat (CRISPR)-Cas9 gene editing, RPE1 cells were transfected with a vector expressing the single guide RNA (sgRNA), targeting *TULP3*, CAS9, and a puromycin resistance cassette (Ran et al., 2013). The following day, cells were treated with 10 μg/ml of puromycin. After 5 d of puromycin treatment, cells underwent limiting dilution cloning, and clones were screened for the predicted *TULP3* knockout.

Constructs. Mouse SSTR3-expressing constructs were derived from a previously used SSTR3-mKate2 construct (Chadha et al., 2019). To generate SSTR3-iRFP670 (referred to as SSTR3-670), the mKate2 tag was replaced with the iRFP670 tag. The constructs SSTR3-Ct1–4 were progressive C-terminal deletions of Avi-SSTR3-EGFP, with SSTR3-Ct4 being the shortest of the series. In SSTR3-Ct4, amino acids 338–428 of SSTR3 were excised, so that a short linker (GSGGSIAT) followed the sequence, SYRFKQGFRRIL, which occurs after the juxtamembrane region, immediately before the EGFP tag. SSTR3 Ct1-3 had the same vector design, with more of the C terminus of SSTR3 (see Fig. 2*A*). Avi-SSTR3 and Avi-SSTR3-Ct4 (see Fig. 2*F*) were generated by removing the EGFP tag from the corresponding EGFP-labeled constructs. Bovine rhodopsin-expressing vectors were derived from constructs used in Chadha et al. (2019). RHO-EGFP-C8 contained a repeat of the last eight amino acids of RHO, ETSQVAPA. Avi-RHO^{1-314}-SCt1 and Avi-RHO^{1-314}-SCt9 were generated by removing the last 34 amino acids from the C terminus of the Avi-RHO construct, following the amino acids FR, and adding the SCt1 sequence (SYRFKQGFRRILLRPSRRIRSQEPGSGPPEKT) or SCt9 sequence (FKQGFRRILLRPSRRIRSQE). Avi-RHO^{1-314}-SCt1-EGFP and Avi-RHO^{1-314}-SCt9-EGFP also contained a short linker (LRSGG) before the EGFP tag. The human CD8A-EGFP plasmid was a gift from Lei Lu (plasmid #86051, Addgene; Madugula and Lu, 2016). All CD8A-EGFP chimeras, including those used for alanine scanning mutagenesis, were generated by the addition of amino acid sequences (see Fig. 3*C*,*D*), immediately after the EGFP tag of CD8A-EGFP (e.g., CD8a-EGFP-SCt9 from Fig. 3*C* was CD8a-EGFP-FKQGFRRILLRPSRRIRSQE). pDisplay-BirA-ER was a gift from Alice Ting (plasmid #20856, Addgene; Howarth et al., 2005). Vector schematics are displayed using Protter (ETH Zurich). EGFP-EHD1 (Eps15 homology-domain containing protein 1) was a gift from Chris Westlake (Lu et al., 2015). The MKS1-mEmerald construct was a gift from Michael Davidson (plasmid #54183, Addgene.

For subretinal electroporation, RHO-EGFP, SSTR3-EGFP, and RHO^{1-314}-SCt1-EGFP constructs were generated by PCR amplification of the respective constructs in a vector containing a 2.5 kb human *RHO* promoter. RHO^{1-314}-EGFP was generated by excision of the 32-amino-acid SCt1 tag, which was flanked by a pair of AccIII restriction sites, and RHO^{1-340}-EGFP was generated by insertion of a PCR product corresponding to $RHO^{315-340}$ following RHO^{1-314}. CD8a-EGFP and CD8a-EGFP-SCt1 were generated by PCR amplification of the respective constructs used for *in vitro* studies. CD8a-EGFP-RhoCt was generated by inserting the last 38 amino acids of RHO following the EGFP tag of CD8a-EGFP. These CD8a-based constructs were also driven by the 2.5 kb human *RHO* promoter.

TULP3 knockout was performed by transfection of hTERT-RPE1 cells with the PX459 vector (PX459 was a gift from Feng Zhang; plasmid # 48139, Addgene; Ran et al., 2013), containing both Cas9 and the sgRNA GGAGTATGACAGTTCACCAA targeting *TULP3* (Han et al., 2019). For rescue experiments, we purchased a gene block (Integrated DNA Technologies) with the coding region of TULP3. We inserted this segment into an mKate2-expressing vector to generate mKate2-TULP3.

Cilium to plasma membrane fluorescence intensity ratio measurements. Cilium to plasma membrane fluorescence intensity ratio (CPIR) measurements were performed on a Nikon Eclipse Ti2-E inverted

microscope with 60× 1.40 numerical aperture (NA) Plan Apo oil immersion objective, dual Andor iXon 888 EMCCD cameras, and a Yokogawa high-speed CSU-X1 spinning disk, using a methodology that was described previously (Geneva et al., 2017; Chadha et al., 2019). Representative 2 × 2 pixel squares along the central line of the cilium were picked and averaged to measure observed cilium fluorescence in ImageJ software. The background fluorescence in the same Z plane was measured and subtracted to obtain actual cilium fluorescence. This was normalized to the actual florescence in the apical membrane of the cell to obtain a CPIR value.

In many cases, IMCD3 cilia protrude vertically from the apical surface of the cell. However, given that the orientation of the cilium is important for consistent CPIR values (Geneva et al., 2017), cilia were only quantified when they were aligned horizontally, that is, lying on the apical surface. Geneva et al. (2017), modeled this position to be the equivalent of a cylinder lying on a planar surface. Thus, they calculated that when the concentration of a fluorescent protein is the same in the ciliary and apical membranes, the cilium should appear 2.3 times brighter. However, the apical membrane of polarized IMCD3 cells, like that of other epithelia, may not be planar because of the presence of microvilli. Although microvilli are likely to be quite limited in the cells of the present study because the cells were grown on coverslips (cf. Pihakaski-Maunsbach et al., 2010), we have avoided assumptions about the organization of the apical membrane by using the CPIR only as a relative measurement. We used the apparent fluorescence intensity in the ciliary membrane versus that in the apical plasma membrane to compare ciliary localization among different fluorescent proteins in the same cell type.

Structured illumination microscopy imaging. Three-dimensional structured illumination microscopy (SIM) imaging was performed using a GE OMX SR microscope with a Blaze SIM module, 60× 1.42 NA point spread function objective lens and pco.edge sCMOS cameras. Z planes were obtained 125 nm apart, and we collected 15 raw images per plane (three angles and five phases). Reconstructions were performed with a Wiener filter setting of 0.001, along with channel-specific optical transfer functions in the softWoRx software package (Applied Precision). Wide-field reference images were wide-field reconstructions of 3D SIM datasets generated in softWoRx. Live imaging at 37°C was performed using oil with a refractive index of 1.524, and experiments at room temperature were performed using oil with a refractive index of 1.518.

Alignment of the reconstructed images was confirmed using tetraspeck beads imaged near the plane of the cilium. For some images, the green channel was Z shifted by 250 nm relative to the far-red channel to compensate for the difference in the Z position of green and far-red fluorophores that was observed with tetraspeck beads.

For analysis of SIM images, 3D reconstructions were imported into ImageJ. The base of the cilium was defined using a cilium-specific label, and a line profile was generated perpendicular to the cilium at that point. The line profile was imported into OriginPro (OriginLab) and fitted to multiple Gaussian distribution curves with the Peak Analyzer tool, using the second derivative of the line profile to search for hidden peaks in the line profile. Curve peaks were obtained and used to determine the percentage of fluorescence from the ciliary membrane relative to the sum of that from the cilium and ciliary pocket.

Western blot. hTERT-RPE1 cells were lysed in RIPA buffer, containing PMSF and protease inhibitor cocktail. Lysed cells were centrifuged at 10,000 × *g* for 10 min to remove debris, and the supernatant was collected. Protein concentration was obtained using the Pierce Micro BCA kit (Thermo Fisher Scientific). We loaded 10 µg of protein lysate of wild-type or *TULP3* knockout lines in each lane. Western blots were probed with a 1:200 dilution of rabbit anti-TULP3 (catalog #13 637–1-AP, Proteintech) and 1:5000 mouse anti-GAPDH (Invitrogen). TULP3 antibody was validated by visual inspection of a Western blot in which one major band was identified at the correct size from wild-type hTERT-RPE1 lysate.

Immunofluorescence. For labeling of TCTN2, hTERT-RPE1 cells were methanol fixed at −20°C for 3 min, washed in 0.1 M phosphate buffer, blocked in 5% goat serum with 1% BSA and 0.1% TX-100, and treated with a 1:200 dilution of rabbit anti-TCTN2 (catalog #17 053–1-AP, Proteintech) overnight at 4°C before secondary staining. The TCTN2 antibody has been validated for immunofluorescence in previous studies of the ciliary transition zone (Garcia-Gonzalo et al., 2011).

For cilium labeling (see Fig. 8*B–D*), hTERT-RPE1 cells were fixed in 4% formaldehyde, 0.1 M phosphate buffer for 10 min, washed in 0.1 M phosphate buffer to remove fixative, blocked using the same blocking buffer described above, and stained with a 1:500 dilution of YF594-conjugated acetylated tubulin antibody (catalog #YF594-66 200, Proteintech) for 1 h at room temperature before washing.

Electron microscopy. hTERT-RPE1 cells were fixed with 2% formaldehyde and 2% glutaraldehyde in 0.1 M cacodylate buffer, pH 7.4, at 4°C for 24 h and postfixed during 2 h in darkness with 1% OsO_4 (w/v) diluted in ultrapure water. Then, cells were washed with distilled water and dehydrated using a graded ethanol series and a final step in propylene oxide before resin infiltration. Samples were subsequently embedded in Araldite 502 resin (Electron Microscopy Sciences), and ultrathin sections were obtained using a PowerTome X ultramicrotome (RMC Boeckeler). Sections were contrasted with uranyl acetate and lead citrate and were analyzed using a JEM-1400 Plus (JEOL) electron microscope with an Orius SC1000A (Gatan) camera with Gatan Microscopy Suite Software. Minor contrast and brightness adjustments to whole images were performed with Adobe Photoshop CS6 software. Length and width measurements were conducted with ImageJ software.

Mice. Animal use followed National Institutes of Health guidelines with an approved protocol. Mice were kept on a 12 h light/12 h dark cycle under 10–50 lux of fluorescent light during the light cycle. We used CD1 mice that were randomized according to sex for our studies.

Subretinal electroporation, retinal dissection, and imaging of photoreceptors. We injected 2–3 µg/µl DNA solution, containing a plasmid-expressing EGFP-tagged proteins under the 2.5-kb human *RHO* promoter, into the subretinal space of CD1 mice using a FemtoJet 4i system (Eppendorf), followed by electroporation with an ECM 830 Square Wave Electroporation System (BTX). Mice were killed at P 21, the eyes were enucleated, and after immersion in fixative 4% formaldehyde in 0.1 M phosphate buffer, corneas were punctured. After 2 h, each eye was dissected, and the retinal pigment epithelium was mechanically separated from the neural retina. A flatmount of the retina was then imaged using a Nikon Eclipse Ti2-E inverted microscope with NIS-Elements software (Nikon). Three-dimensional stacks of photoreceptors were imaged at an interval of 0.3 µm, and an orthogonal view was taken of the resulting volume using the 3-D viewer in NIS-Elements software. The localization of the outer segment layer was confirmed by colabeling with wheat germ agglutinin (WGA)-647. For measurements of the percentage of fluorescence in the OS, we measured the average fluorescence of representative regions of the outer segment and inner segment (IS) from orthogonal views, subtracted any background fluorescence, and divided the OS fluorescence by the IS+OS fluorescence.

Experimental design and statistical analysis. We performed all *in vitro* experiments on multiple cultures. For CPIR measurements, experiments were repeated until an *n* value of ~20 cilia was achieved. For quantitative 3-D SIM measurements, experiments were repeated until an *n* value of ~15 was achieved. We tested datasets for normality using the Kolmogorov–Smirnov test. As all datasets were observed to be at least partly composed of non-normally distributed data, multiple comparisons were performed using the nonparametric Kruskal–Wallis test, followed by Dunn's multiple comparisons test. Single comparisons were performed using the Mann–Whitney *U* test. All statistical tests were two sided.

Results

Relative localization of RHO and SSTR3 to different types of primary cilia

As reported previously, SSTR3 localizes very specifically to the cilium of IMCD3 cells (Berbari et al., 2008a; Hu et al., 2010; Ye et al., 2013; Geneva et al., 2017). RHO has also been shown to localize to IMCD3 cilia (Wang et al., 2012; Wang and Deretic, 2015),

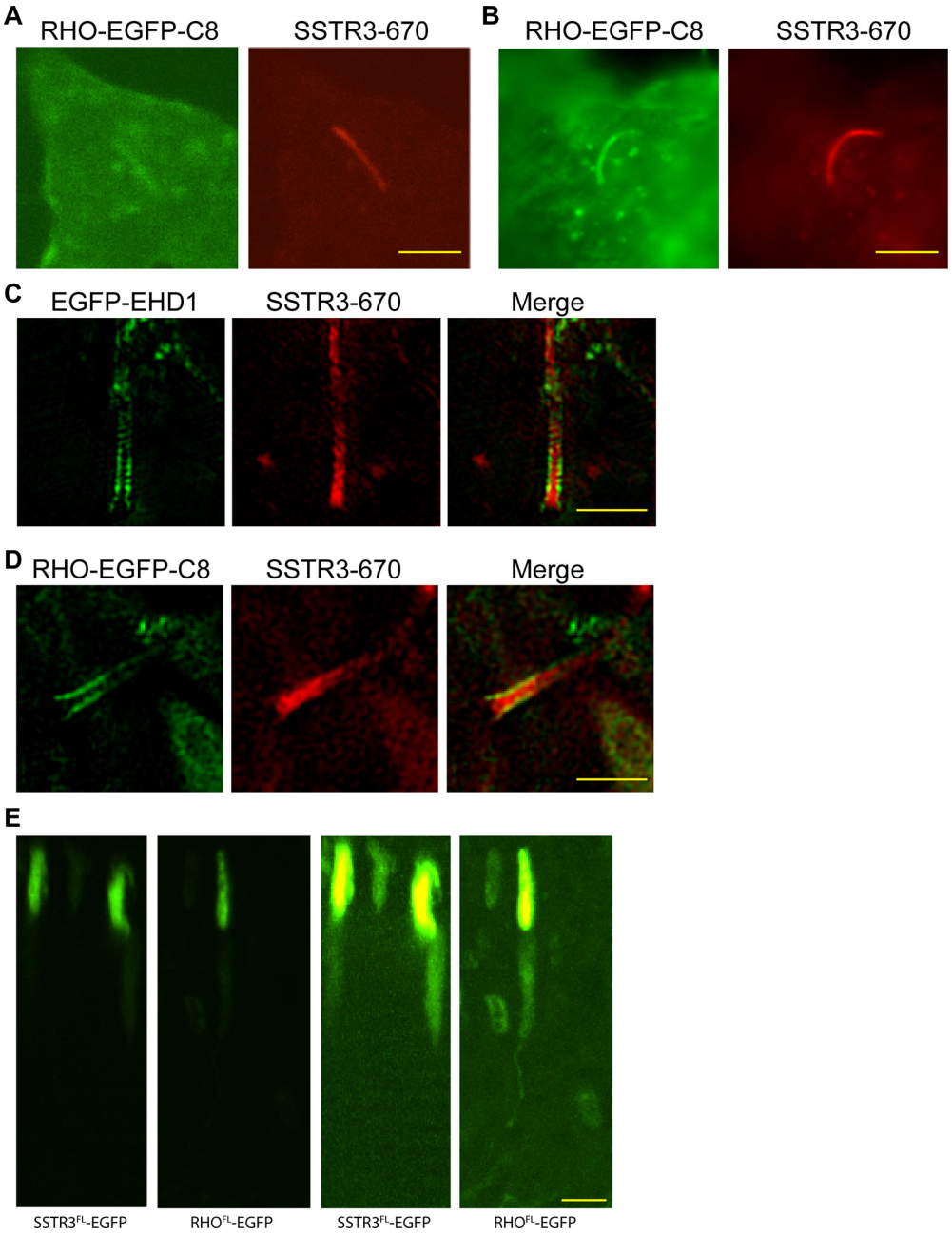

Figure 1. Comparison of RHO and SSTR3 localization in cilia of IMCD3, hTERT-RPE1, and photoreceptor cells. ***A***, RHO-EGFP-C8 and SSTR3-mKate2 labeling of the same cilium of an IMCD3 cell, imaged by spinning disk confocal microscopy; the RHO labeling of the cilium is not as specific as the SSTR3-mKate2 labeling. Scale bar, 5 μm. ***B***, RHO-EGFP-C8 and SSTR3-mKate2 labeling of the same cilium in an hTERT-RPE1 cell, imaged by spinning disk confocal microscopy; the RHO labeling of the cilium is not as specific as the SSTR3-mKate2 labeling. Scale bar, 5 μm. ***C***, Three-dimensional SIM imaging of EGFP-EHD1, a marker for the periciliary membrane (Lu et al., 2015). Scale bar, 2 μm. ***D***, RHO-EGFP-C8 and SSTR3-mKate2 labeling of the same cilium in an hTERT-RPE1 cell, imaged by 3D SIM; in this example, the RHO is localized mainly to the periciliary membrane, surrounding the cilium membrane region, which is labeled by SSTR3-mKate2. Scale bar, 2 μm. ***E***, Orthogonal view of retinal flatmounts from mice that had been electroporated with either SSTR3-EGFP or RHO-EGFP. The overall brightness of the image is increased in right panels to make the dim IS fluorescence visible. Scale bar, 5 μm.

but the specificity of ciliary localization was significantly lower for RHO compared with SSTR3 (Geneva et al., 2017; Chadha et al., 2019). We confirmed these reports using SSTR3-670, together with the RHO-EGFP-C8 construct, which features a repeat of the last eight residues, ETSQVAPA, including the VXPX motif (Fig. 1*A*).

Another cell line that has been used for heterologous expression studies on primary cilia is the hTERT-RPE1 line. The cilia of hTERT-RPE1 cells extend from a pocket, unlike 90% of IMCD3 cilia, which emerge directly from the cell surface (Molla-Herman et al., 2010). Therefore, the basal region of the cilium is surrounded by a closely apposed periciliary membrane. A particular interest in this type of cilium is that the basal organization bears some similarity to the basal region (i.e., the connecting cilium) of the photoreceptor cilium (i.e., the OS; Trivedi et al., 2012). The photoreceptor cilium is rooted in the IS so that the base of the cilium is partially surrounded by the inner segment, forming a partial pocket (Liu et al., 2007, their Fig. 3*C*). The periciliary membrane of the inner segment appears to be a site of docking for RHO vesicles, migrating from the Golgi in the IS (Papermaster et al., 1985; Deretic and Papermaster, 1991); in frog rod photoreceptors, with high volume of traffic into

the cilium, the periciliary membrane is amplified into a series of folds, known as the periciliary ridge complex (Peters et al., 1983).

Spinning disk confocal microscopy indicates that SSTR3-670 localizes very specifically to the RPE1 cilium, comparable to previous reports in the IMCD3 cilium (Mukhopadhyay et al., 2010; Tian et al., 2014; Madugula and Lu, 2016). Although not to the same extent as in the IMCD3 cells, RHO-EGFP-C8 labeling was also evident generally in the plasma membrane, indicating less cilium specificity than that for SSTR3-670 (Fig. 1*B*). Using super-resolution microscopy, an additional distinction between SSTR3 and RHO localization was evident. SIM allowed for the resolution of the ciliary membrane and the periciliary membrane as separate structures. EHD1 has been shown to be localized to the periciliary membrane of hTERT-RPE1 cells (Lu et al., 2015). SSTR3-670 (or -EGFP) was localized almost exclusively inside EGFP-EHD1 labeling, indicating localization to the ciliary plasma membrane and exclusion from the periciliary membrane (Fig. 1*C*). RHO-EGFP-C8 showed considerable variation from cell to cell but could be detected in the periciliary membrane of some cilia, with sometimes the majority of the signal coinciding with this outer structure and thus surrounding the SSTR3 signal (Fig. 1*D*; see below for quantification of localization).

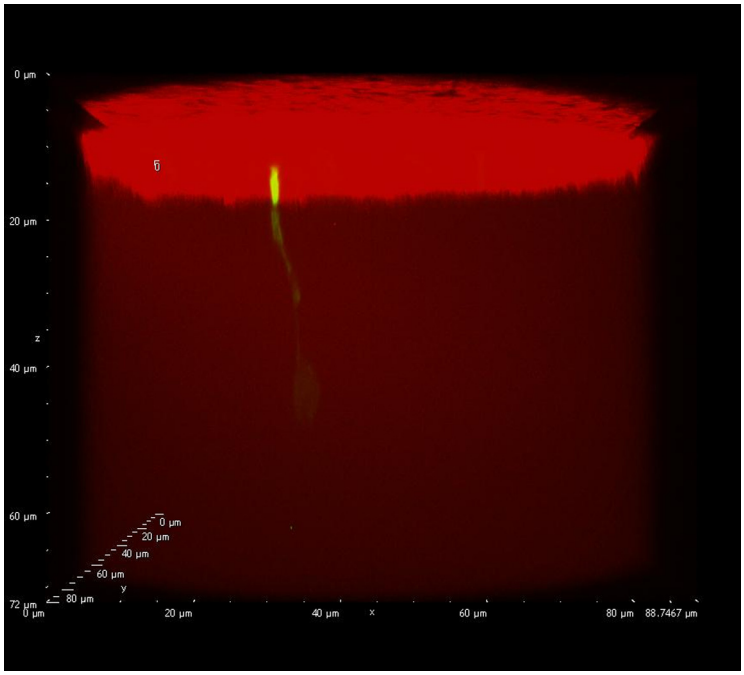

Movie 1. Retinal flatmounts were imaged to generate 3D volumes, which enabled comparison of IS and OS fluorescence. WGA-647 was used to confirm the localization of the OS layer. [View online]

Given the greater enrichment of SSTR3 compared with RHO in IMCD3 and RPE1 cilia, one might expect the converse of these findings in rod photoreceptor cilia, which normally contain a high concentration of RHO. To address this question, we performed subretinal electroporation of WT mice and studied the localization of SSTR3-EGFP and RHO-EGFP in the photoreceptor cilium by examining orthogonal views from Z stacks of flatmounts from electroporated retinas (Movie 1). As expected, RHO-EGFP was primarily localized to the OSs of rod photoreceptors. However, SSTR3-EGFP was also localized to rod outer segments; indeed, fluorescence intensity suggested that it localized nearly as well as RHO-EGFP (Fig. 1*E*).

These observations indicate that SSTR3 possesses a CLS that is highly effective in a broad range of primary cilia, from the simple IMCD3 cilium to the pocket cilium of RPE1 cells to the most elaborate of all cilia, the highly specialized photoreceptor cilium. RHO, on the other hand, possesses a CLS that appears to function relatively better in rod photoreceptor cells.

Requirement of motif in C terminus of SSTR3 for cilium localization in IMCD3 cells

Berbari et al., (2008a) reported that replacement of the well-characterized third intracellular loop (IC3) of SSTR3 with the IC3 of SSTR5, which does not localize to a cilium, did not prevent ciliary localization. These authors therefore suggested that there may be one or more additional CLSs in SSTR3. Given the presence of C-terminal CLSs in other GPCRs, such as RHO, and especially SMO, which contains considerable C-terminal homology with the C terminus of SSTR3 (Corbit et al., 2005), we tested the role of the C terminus of SSTR3 in ciliary trafficking.

First, we generated EGFP-tagged SSTR3 constructs with progressive deletions of the C terminus of the protein (whose full length is 428 amino acids): SSTR3-Ct1 (1–357), SSTR3-Ct2 (1–348), SSTR3-Ct3 (1–346) and SSTR3-Ct4 (1–337; Fig. 2*A*). To study the relative ciliary localization among different proteins, we used the cilium to plasma membrane (fluorescence) intensity ratio, which we and others have used in previous studies to quantify ciliary localization (Madugula and Lu, 2016; Geneva et al., 2017; Chadha et al., 2019). When the C terminus of SSTR3 was truncated, protein was still detected in the cilium (Fig. 2*B*), however, we observed substantially reduced CPIR values, particularly when the region close to the initial portion of the C terminus was perturbed, as with SSTR3-Ct4 (Fig. 2*C*).

Previous studies have indicated that the presence of an EGFP tag may affect ciliary localization (Madugula and Lu, 2016). Hence, we tested SSTR3 chimeras that instead of having a C-terminal EGFP, were N-terminally tagged with a 15-amino-acid biotin acceptor peptide (avitag), and subsequently treated with streptavidin-Alexa Fluor 488. Similar to our result with SSTR3-EGFP, the ciliary localization of Avi-SSTR3 was reduced significantly by a deletion of the majority of the SSTR3 C terminus, as in Avi-SSTR3-Ct4 (Fig. 2*F*,*G*).

We next tested whether the SSTR3 C terminus could promote ciliary localization of proteins that are typically less concentrated than SSTR3 in the cilia of transfected IMCD3 cells. This approach provides a test of sufficiency of the C-terminal CLS in the absence of the remainder of the SSTR3 protein, including the CLSs in the IC3 loop (Berbari et al., 2008a). The ciliary concentration of RHO, with or without a tag, is less than that of SSTR3 (Geneva et al., 2017; Chadha et al., 2019) (Fig. 1*A*). As shown in Figure 2, *F* and *G*, we measured a significant increase in the CPIR with IMCD3 cells, when we replaced the C-terminal 34 amino acids of Avi-RHO with either the Ct1 of SSTR3 (SCt1), or SCt9, which we determined to be the minimal CLS from the SSTR3 C terminus when appended to CD8A-EGFP.

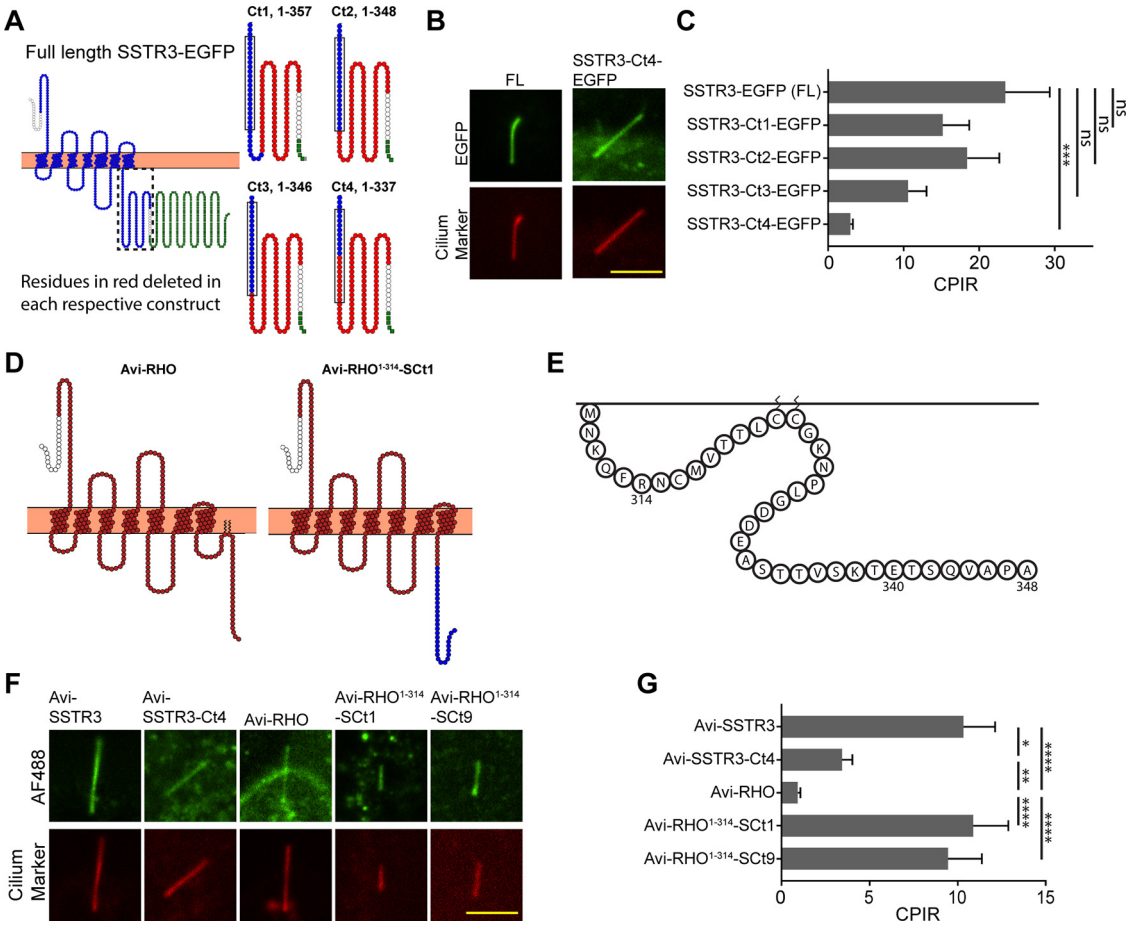

Figure 2. Novel CLS in SSTR3, demonstrated with live IMCD3 cells. ***A***, Schematic of full-length Avi-SSTR3-EGFP and derived truncation constructs (corresponding to region indicated by dotted black line). Blue indicates SSTR3 sequence, green indicates EGFP sequence, and red indicates amino acids of the full-length sequence that were removed in each truncation. Solid black rectangle indicates 20 amino acid sequence that we ultimately determined to be critical for ciliary localization. White residues represent the linker sequence GSGGSIAT. ***B***, Representative images showing fluorescence from full-length (FL) Avi-SSTR3-EGFP, compared with a truncation in which only 32 amino acids of the C terminus of SSTR3 remained (SSTR3-Ct4). The presence of SSTR3-Ct4 on the plasma membrane reflects a reduced ciliary enrichment. Full-length SSTR3-iRFP670 was used as a cilium marker. Scale bar, 5 μm. ***C***, CPIR of full-length versus SSTR3 truncations. Note that all constructs also included an N-terminal avitag, however only EGFP fluorescence was analyzed for these experiments; $n = 16–26$. Means ± SEM. ***$p < 0.001$, Kruskal–Wallis test with *post hoc* Dunn's multiple comparisons test. ***D***, Schematic of full-length Avi-RHO and Avi-RHO$^{1-314}$-SCt1 in which the 34 C-terminal amino acids of RHO were replaced with 32 amino acids from the SSTR3 C terminus. ***E***, Schematic of the 34 C-terminal amino acids of bovine RHO. RHO 314, 340, and 348 are indicated. ***F***, Representative images of avitag-labeled SSTR3, SSTR3-Ct4, RHO, RHO$^{1-314}$-SCt1 (in which the C-terminal 34 amino acids of RHO were replaced with 32 amino acids from the SSTR3 C terminus) and RHO$^{1-314}$-SCt9 (which contains a 20-amino-acid sequence from the SSTR3 C terminus), following treatment with streptavidin Alexa Fluor 488. SSTR3-iRFP670 was used as a cilium marker. Scale bar, 5 μm. ***G***, CPIR values measured, using constructs that only included an avitag (no EGFP). For these experiments, cells were cotransfected with biotin ligase, grown in 10 μM biotin solution and treated with streptavidin-Alexa Fluor 488 before imaging. **$p < 0.01$, Mann–Whitney test, $n = 17–35$.

To characterize the CLS property of the SSTR3 C-terminal region of SSTR3 in detail, we used CD8A-EGFP chimeras, to which we appended CLS candidates from the SSTR3 C terminus. CD8A is a single-pass transmembrane protein (Fig. 3*A*), and chimeras of CD8A have been used successfully in several studies of ciliary localization tags (Follit et al., 2010; Madugula and Lu, 2016; Badgandi et al., 2017). The difference between these experiments and those involving SSTR3 C terminus deletion is that these test whether the SSTR3 C-terminus, in isolation from the IC3 loop, is sufficient for driving ciliary localization (Berbari et al., 2008a).

Whereas CD8A-EGFP is minimally present in the cilium (Fig. 3*B*,*C*), addition of an SSTR3 C-terminal CLS results in robust enrichment in the cilium (Fig. 3*C*). We initially examined a 32-amino-acid sequence (CD8A-EGFP-SCt1); this sequence represents the portion of SSTR3 C terminus remaining in the SSTR3-Ct1 deletion (Fig. 2*A*,*C*). Addition of this 32-amino-acid sequence effected enrichment in the cilium, indicating that this region of the C terminus of SSTR3 contains a ciliary localization sequence sufficient to impart localization of CD8A-EGFP to the cilium (Fig. 3*C*).

We sought to define the minimal CLS sufficient for ciliary localization, following the approach performed with studies on the fibrocystin CLS (Follit et al., 2010) and the polycystin-1 CLS (Luo et al., 2019). We initially trimmed the C terminus of the CD8A-EGFP-SCt1 construct and found that trimming the motif beyond the QE sequence at the C terminus resulted in a large reduction in ciliary localization. When we trimmed the SCt6 tag at the N-terminal end, we observed that removal of residues beyond the FK sequence also resulted in a reduction in ciliary localization, in agreement with a previous prediction (Fig. 3*C*; Corbit et al., 2005). Therefore, these studies demonstrate that the minimal ciliary localization sequence in the SSTR3 C terminus is the 20-amino-acid sequence from 329–348, FKQGFRRILLRPSRRIRSQE.

Recent studies have suggested the presence of a charge code for ciliary localization of peripheral membrane proteins (Maza et al., 2019), raising the possibility that charge might also be

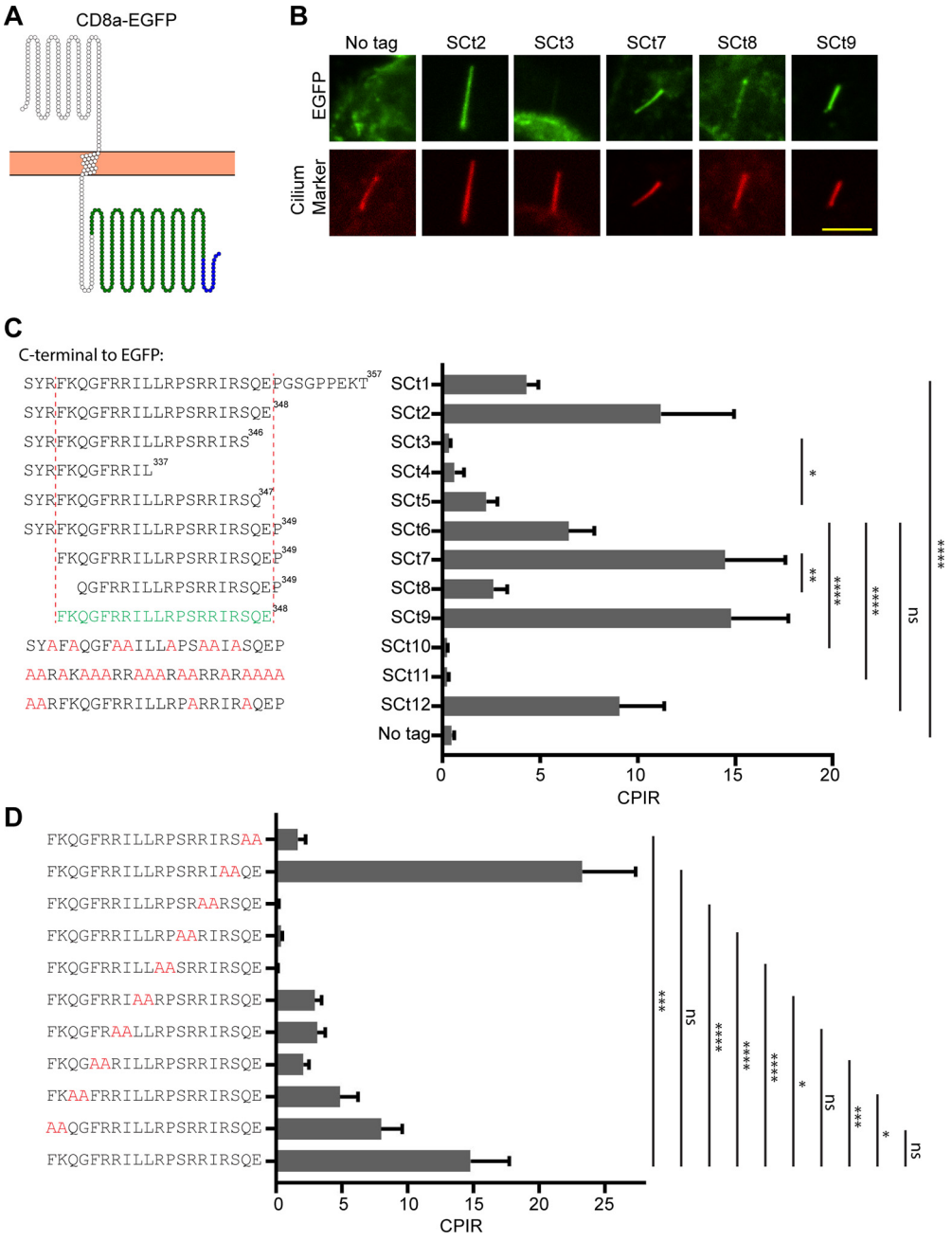

Figure 3. Characterization of the SSTR3 C terminus CLS by addition to CD8A in IMCD3 cells. ***A***, Schematic of CD8A chimeric protein. Green indicates EGFP. Blue indicates the location where each CLS was added. ***B***, Representative images showing fluorescence from CD8A-EGFP (no tag), and chimeras containing SSTR3 amino acids 326–348 (SCt2), 326–346 (SCt3), 329–349 (SCt7), 331–349 (SCt8), and 329-348 (SCt9). They demonstrate that SSTR3 329-348 (SCt9) is the minimal sequence sufficient to enable robust ciliary localization of CD8A-EGFP. Scale bar, 5 μm. ***C***, CPIRs of various SSTR3 C-terminal CLS variants appended to CD8A-EGFP. The sequences of SCt1-12 are shown on the left. SCt 1–4 correspond to the sequences remaining in the SSTR3 C terminus in Figure 2*A*. Red dotted line and sequence in green (SCt9) indicate the minimal 20-amino-acid functional SSTR3 CLS; $n = 15–29$. *$p < 0.05$, **$p < 0.01$, ****$p < 0.0001$, Kruskal–Wallis test with *post hoc* Dunn's multiple comparisons test. ***D***, Pairs of amino acids in SCt9 that were mutated to alanine and compared for the effect of amino acids on CPIR; $n = 17–32$.

important for the localization of other ciliary membrane proteins. The C-terminal CLS of SSTR3 is rich in positively charged amino acids, with the net charge potentially regulated by phosphorylation (Lehmann et al., 2016). To test whether amino acid charge might affect ciliary localization of SSTR3, we first modified the nonpositively charged residues to Ala. This alteration resulted in a large reduction in ciliary localization, as did mutation of the positively charged residues to Ala (compare SCt6 with SCt10 and SCt11; Fig. 3*C*). Therefore, the positively charged residues in the SSTR3 CLS are required but not sufficient for ciliary localization. Mutation of the phosphorylation residues of the SSTR3 CLS to Ala did not result in a significant reduction in CPIR values (compare SCt6 with SCt12; Fig. 3C), suggesting that phosphorylation likely plays a minimal role in localization of this sequence to the cilium. A compilation of mean CPIR measurements for different constructs expressed in IMCD3 cells is shown in Table 1.

Alanine scanning mutagenesis is a useful tool for defining important residues in a ciliary localization sequence (Follit et al., 2010; Luo et al., 2019). We performed an Alanine scan of the 20-amino-acid SSTR3 CLS and found that although the majority of the sequence was important for ciliary localization, the sequence

Table 1. Relative ciliary localization of different proteins in IMCD3 cells and hTERT-RPE1 cells

Construct	C-terminal domain	IMCD3 CPIR (*n*/experiments)[b]	RPE1 % in cilium membrane[a] (*n*/experiments)[b]
EGFP-EHD1			
SSTR3-EGFP	Full-length SSTR3	23.4 ± 5.9 (16/2)	89.7 ± 2.8 (28/3)
SSTR3-SCt1-EGFP	SYRFKQGFRRILLRPSRRIRSQEPGSGPPEKT	15.2 ± 3.5 (28/2)	
SSTR3-SCt2-EGFP	SYRFKQGFRRILLRPSRRIRSQE	18.4 ± 4.3 (19/2)	
SSTR3-SCt3-EGFP	SYRFKQGFRRILLRPSRRIRS	10.6 ± 2.4 (21/2)	
SSTR3-SCt4-EGFP	SYRFKQGFRRIL	2.9 ± 0.3 (26/2)	56.6 ± 6.7 (45/8)
Avi-SSTR3	Full-length SSTR3	10.3 ± 1.9 (35/4)	
Avi-SSTR3-SCt4	SYRFKQGFRRIL	3.4 ± 0.6 (22/2)	
CD8A-EGFP		0.5 ± 0.1 (21/2)	15.5 ± 7 (16/2)
CD8A-EGFP-SCt1	SYRFKQGFRRILLRPSRRIRSQEPGSGPPEKT	4.3 ± 0.6 (29/3)	100 (16/2)
CD8A-EGFP-SCt2	SYRFKQGFRRILLRPSRRIRSQE	11.9 ± 3.8 (21/3)	
CD8A-EGFP-SCt3	SYRFKQGFRRILLRPSRRIRS	0.3 ± 0.1 (15/2)	0 (7/2)
CD8A-EGFP-SCt4	SYRFKQGFRRIL		
CD8A-EGFP-SCt5	SYRFKQGFRRILLRPSRRIRSQ	2.2 ± 0.6 (21/3)	
CD8A-EGFP-SCt6	SYRFKQGFRRILLRPSRRIRSQEP	6.5 ± 1.3 (20/3)	
CD8A-EGFP-SCt7	FKQGFRRILLRPSRRIRSQEP	14.5 ± 3.1 (25/2)	
CD8A-EGFP-SCt8	QGFRRILLRPSRRIRSQEP	2.6 ± 0.7 (20/2)	
CD8A-EGFP-SCt9	FKQGFRRILLRPSRRIRSQE	14.8 ± 2.9 (24/2)	
CD8A-EGFP-SCt10	SYAFAQGFAAILLAPSAAIASQEP	0.2 ± 0.04 (24/2)	
CD8A-EGFP-SCt11	AARAKAAARRAAARAARRARAAAA	0.2 ± 0.07 (23/2)	
CD8A-EGFP-SCt12	AARFKQGFRRILLRPARRIRAQEP	9.1 ± 2.3 (29/2)	
CD8A-EGFP-SCt9-Ala1	FKQGFRRILLRPSRRIRSAA	1.6 ± 0.6 (20/2)	
CD8A-EGFP-SCt9-Ala2	FKQGFRRILLRPSRRIAAQE	23.2 ± 4.0 (24/2)	
CD8A-EGFP-SCt9-Ala3	FKQGFRRILLRPSRAARSQE	0.2 ± 0.04 (20/2)	
CD8A-EGFP-SCt9-Ala4	FKQGFRRILLRPAARIRSQE	0.4 ± 0.07 (22/2)	
CD8A-EGFP-SCt9-Ala5	FKQGFRRILLAASRRIRSQE	0.10 ± 0.03 (23/2)	
CD8A-EGFP-SCt9-Ala6	FKQGFRRIAARPSRRIRSQE	2.9 ± 0.5 (25/2)	
CD8A-EGFP-SCt9-Ala7	FKQGFRAALLRPSRRIRSQE	3.1 ± 0.6 (17/2)	
CD8A-EGFP-SCt9-Ala8	FKQGAARILLRPSRRIRSQE	2.1 ± 0.4 (27/2)	
CD8A-EGFP-SCt9-Ala9	FKAAFRRILLRPSRRIRSQE	4.8 ± 1.4 (20/2)	
CD8A-EGFP-SCt9-Ala10	AAQGFRRILLRPSRRIRSQE	8.0 ± 1.6 (32/2)	
RHO-EGFP-C8	Full-length RHO; extra C8 after EGFP		20.5 ± 9.4 (17/3)
RHO1^{-314}-EGFP			97 ± 1.5 (20/4)
RHO1^{-340}-EGFP			27.1 ± 9.8 (17/2)
RHO1^{-314}-SCt1-EGFP	SYRFKQGFRRILLRPSRRIRSQEPGSGPPEKT		93.6 (10/4)
Avi-RHO	Full-length RHO	0.9 ± 0.1 (22/6)	
Avi-RHO1^{-314}-SCt1	SYRFKQGFRRILLRPSRRIRSQEPGSGPPEKT	10.9 ± 2.0 (17/2)	
Avi-RHO1^{-314}-SCt9	FKQGFRRILLRPSRRIRSQE	9.5 ± 1.9 (21/3)	

[a] Percentage of fluorescence on the ciliary membrane, determined by multiple peak fitting of line profiles.
[b] *n*, Number of measurements; experiments, number of discrete experiments for each group.

RPSRRI represented the most sensitive region for ciliary mislocalization (Fig. 3*D*); it had a greater impact on ciliary localization than the FK motif. The QE motif at the end of the construct was also important for ciliary localization, consistent with our observations in Figure 3*C*.

Ciliary versus periciliary membrane localization of SSTR3 and RHO in the pocket cilium of hTERT-RPE1 cells

We next examined the C-terminal CLS of SSTR3 in the context of a pocket cilium. As noted above, the periciliary plasma membrane of the ciliary pocket is closely apposed to the ciliary membrane of hTERT-RPE1 cells (Molla-Herman et al., 2010; Fig. 4*A*), so conventional confocal microscopy cannot resolve the two membranes as separate structures. Hence, we again used SIM to provide enhanced resolution. For these experiments, we labeled the ciliary membrane with SSTR3-670.

As we planned to compare the longer wave length 670 fluorophore with EGFP, we first sought to determine whether a valid comparison could be made between the two fluorophores for the purposes of this SIM experiment. We expressed SSTR3-EGFP and SSTR3-670 in RPE1 cells, and, in support, we observed colocalization of the two signals in the cilium (Fig. 4*C*), indicating no significant deviation because of the different wave lengths. We were also able to resolve the two sides of the ciliary membrane in an optical section, highlighting the utility of SIM for characterizing GPCR localization within cilia (contrast Fig. 4*C*, SIM, and wide-field images).

Wide-field microscopy of cilia that extend out of the pocket and beyond the edge of the cell in the plane of imaging demonstrates that RHO-EGFP-C8 is present in the ciliary plasma membrane (Fig. 4*B*; quantification below). However, as shown above (Fig. 1*D*), SIM imaging showed that RHO-EGFP-C8 labeling could be detected in the periciliary membrane and sometimes appeared to be exclusively localized there; additional examples are shown in Figure 4, *D* and *E*.

We also observed that the periciliary RHO-EGFP-C8 and ciliary SSTR3-670 signals did not meet at the base of the cilium. We imaged live cells expressing MKS1-mEm and SSTR3-670, and observed localization of the transition zone marker proximal to the end of the SSTR3-670 signal (Fig. 4*F*). To further test that the transition zone separates the ciliary and periciliary GPCRs, we immunostained cells expressing RHO-EGFP-C8 and SSTR3-670 for TCTN2, a component of the cilium transition zone (Garcia-Gonzalo et al., 2011; Yang et al., 2015), and observed localization

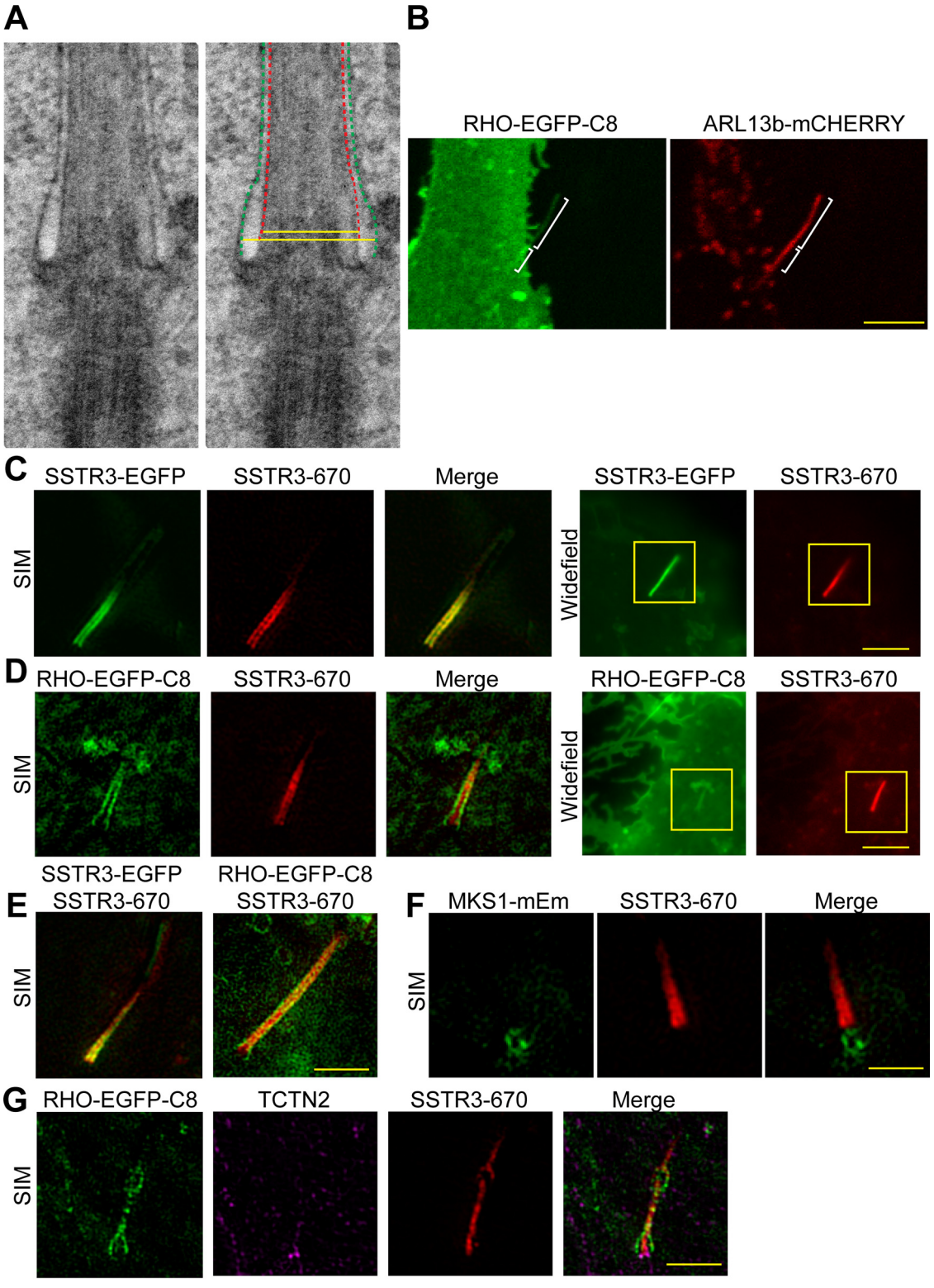

Figure 4. GPCR localization in the pocket cilia of hTERT-RPE1 cells. ***A***, Transmission electron microscopy of a central longitudinal section of the base of a cilium, illustrating the cilium pocket. Right, The pocket membrane in green, and the cilium membrane in red. Yellow lines indicate the maximal diameters of the cilium (210 nm) and the pocket (315 nm). ***B***, Image of a cilium extending beyond the edge of the cell, and thus out of the pocket (large bracket). Presence of RHO-EGFP-C8 in this ciliary extension (left) indicates localization to the ciliary membrane of a live hTERT-RPE1 cell. ARL13b-mCHERRY (right) was used as a cilium marker. Scale bar, 5 μm. ***C***, SIM (left) and wide-field (right) images of the cilium of a live cell expressing SSTR3-EGFP and SSTR3-iRFP670 (written as SSTR3-670). SSTR3-EGFP and SSTR3-iRFP670 both label the cilium membrane, indicating overlap of the green and far-red signals. The area of the SIM images corresponds to the yellow squares in the wide-field images (also in ***D***). Note that SIM images sample a thinner Z slice than that in the wide-field images, causing in this image (and some others), less of the cilium to be visible (because of the distal cilium being out of the image plane). Scale bar, 5 μm. ***D***, SIM and wide-field images of the cilium of a live cell expressing SSTR3-iRFP670, as a ciliary membrane marker, and RHO-EGFP-C8. In this cilium RHO-EGFP-C8 shows localization to the periciliary membrane (pocket). Scale bar, 5 μm. ***E***, Additional examples corresponding to images shown in ***C*** and ***D***. Scale

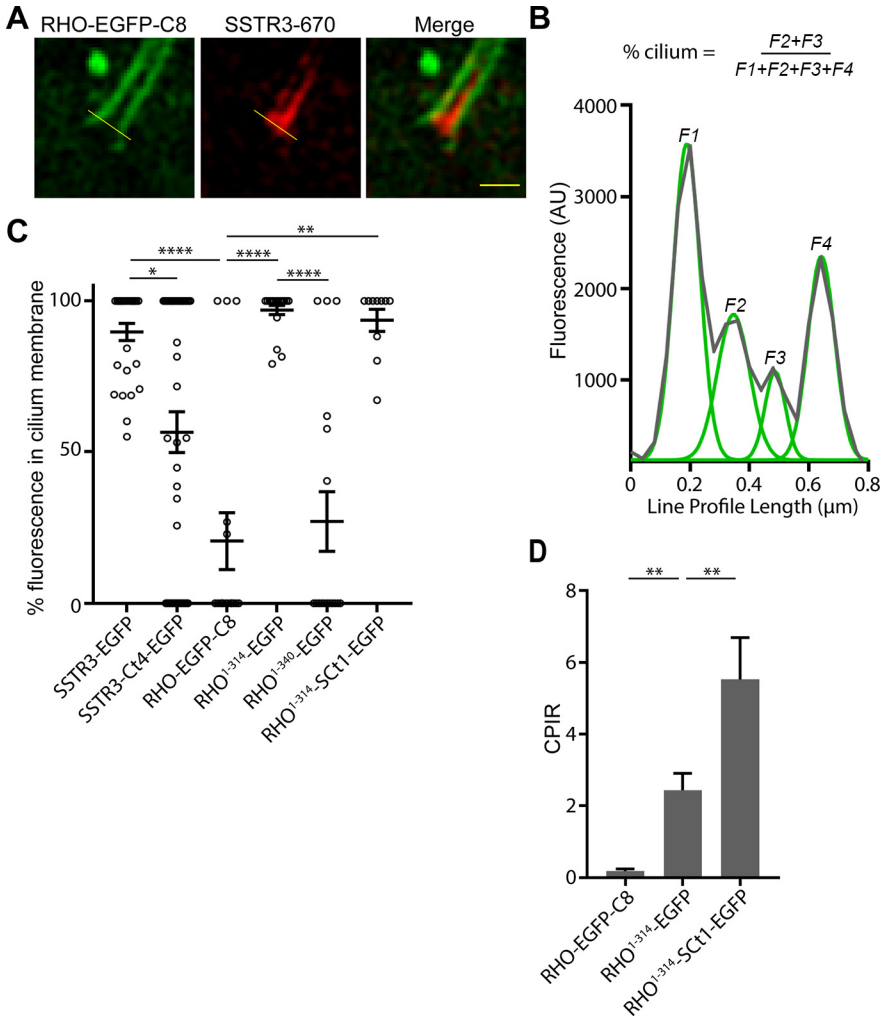

Figure 5. Quantification of fluorescent protein densities in hTERT-RPE1 pocket cilia. ***A***, Image of a cell expressing RHO-EGFP-C8, which in this case appears almost exclusively in the periciliary membrane, and SSTR3-670, which is in the ciliary membrane. Scale bar, 0.5 μm. ***B***, Example of fluorescence line profiles from a cell expressing an EGFP-labeled protein that is present on both the cilium membrane and pocket. Line profile is shown in gray, and Gaussian curve fits are shown in green. Peaks of the Gaussian curves were identified as *F1–4*, and the % of the sum of *F1–4* fluorescence that is from the ciliary membrane (*F2* + *F3*) is represented as the percentage of fluorescence in cilium membrane. ***C***, Comparison of the percentage of fluorescence in ciliary membrane for SSTR3, RHO, and derived proteins, tagged with EGFP; $n = 10–45$. *$p < 0.05$, **$p < 0.01$, ****$p < 0.0001$, Kruskal–Wallis test with *post hoc* Dunn's multiple comparisons test. Error bars indicate means ± SEM. SSTR3-Ct4-EGFP, RHO-EGFP-C8, and RHO$^{1-340}$ show extreme ranges, with localization entirely to the ciliary membrane (100%) in some cases, and localization entirely to the periciliary membrane (0%) in some other cases. For SSTR3-EGFP, 18 of 28 cells had only ciliary fluorescence; the remaining 10 cells exhibited significant fluorescence from the ciliary pocket as well as from the ciliary membrane (cilium fluorescence ranged from 56 to 90% in these cells). In comparison, for RHO-EGFP-C8, 3 of 17 cells exhibited fluorescence that was exclusively from the ciliary membrane, 2 of 17 cells exhibited significant fluorescence from both the ciliary membrane and the pocket (ciliary fluorescence was 21 and 28%), and the remaining 12 cells exhibited only pocket fluorescence. ***D***, CPIRs for RHO-EGFP-C8 (rare cases in which cilium could be observed extending beyond the edge of the cell were used; $n = 5$), RHO$^{1-314}$-EGFP ($n = 38$), and RHO$^{1-314}$-SCt1-EGFP ($n = 39$). For RHO$^{1-314}$-EGFP and RHO$^{1-314}$-SCt1-EGFP, SIM data (***C***) showed mostly ciliary fluorescence, abrogating a need for measuring overhanging cilia. **$p < 0.01$, Kruskal–Wallis test with *post hoc* Dunn's multiple comparisons test.

of TCTN2 in the gap between the periciliary and ciliary membranes (Fig. 4*G*). Therefore, periciliary RHO-EGFP-C8 appears to be separated by the transition zone from the ciliary membrane.

Ciliary versus periciliary membrane localization of SSTR3 and RHO C-terminal mutants and chimeras in hTERT-RPE1 cells

Differences in ciliary versus periciliary localization were clearest near the base of the cilium, where the pocket widens (Fig. 4*A*), and were evident from line profiles of fluorescence at the base of the cilium. Figure 5*A* shows an example of RHO-EGFP-C8, illustrating a line profile used for quantification of protein densities on the pocket and cilium membranes. To quantify the relative fluorescence from the ciliary and ciliary pocket membranes, we fitted our line profiles to Gaussian distribution curves (Fig. 5*B*, green). The sum of the heights of the inner two Gaussian curves (*F2* and *F3*, representing the cilium fluorescence) was expressed as a percentage of the sum of the heights of all four curves (representing the pocket plus cilium fluorescence). From SIM images of RHO-EGFP-C8, the mean percentage of cilium fluorescence was 21 ± 9%, indicating that the fluorescence on the pocket is, on average, about fourfold as bright as the ciliary fluorescence (Fig. 5*C*).

We used quantitative SIM analysis to study the effect of reducing the C terminus of SSTR3 on localization in hTERT-RPE1 pocket cilia. We found that SSTR3-Ct4-EGFP was frequently detected in the periciliary membrane and thus exhibited a significantly lower percentage of fluorescence in the ciliary membrane than SSTR3-EGFP (Figs. 5*C*, 6*A*,*E*), consistent with a role for the C-terminal CLS in enabling movement from the periciliary membrane to the ciliary membrane.

We were interested in whether the SSTR3 C terminal CLS could promote RHO localization to the hTERT-RPE1 cilium membrane, as well as to the IMCD3 cilium membrane (see above). Hence, we sought to replace the C-terminal 34 amino acids of RHO with the 32-amino-acid proximal portion of the SSTR3 C terminus plus EGFP (Fig. 2*A*, Ct1; Fig. 2*D*,*E*, schematics). However, first, we tested the effect of deleting the C-terminal 34 amino acids of RHO-EGFP-C8 to generate RHO$^{1-314}$-EGFP. Surprisingly, RHO$^{1-314}$-EGFP localized to the ciliary membrane (Fig. 6*B*), without any additional C-terminal sequence. Thus, we could not test for a ciliary localization effect

←

bar, 2 μm. ***F***, SIM images of a live cell indicates MKS1-mEmerald labeling the transition zone and SSTR3-670 labeling the ciliary membrane. Scale bar, 2 μm. ***G***, SIM image from a fixed cell expressing RHO-EGFP-C8 and SSTR3-670. Cells were fixed in methanol. The transition zone marker, TCTN2, was immunolabeled. Scale bar, 2 μm.

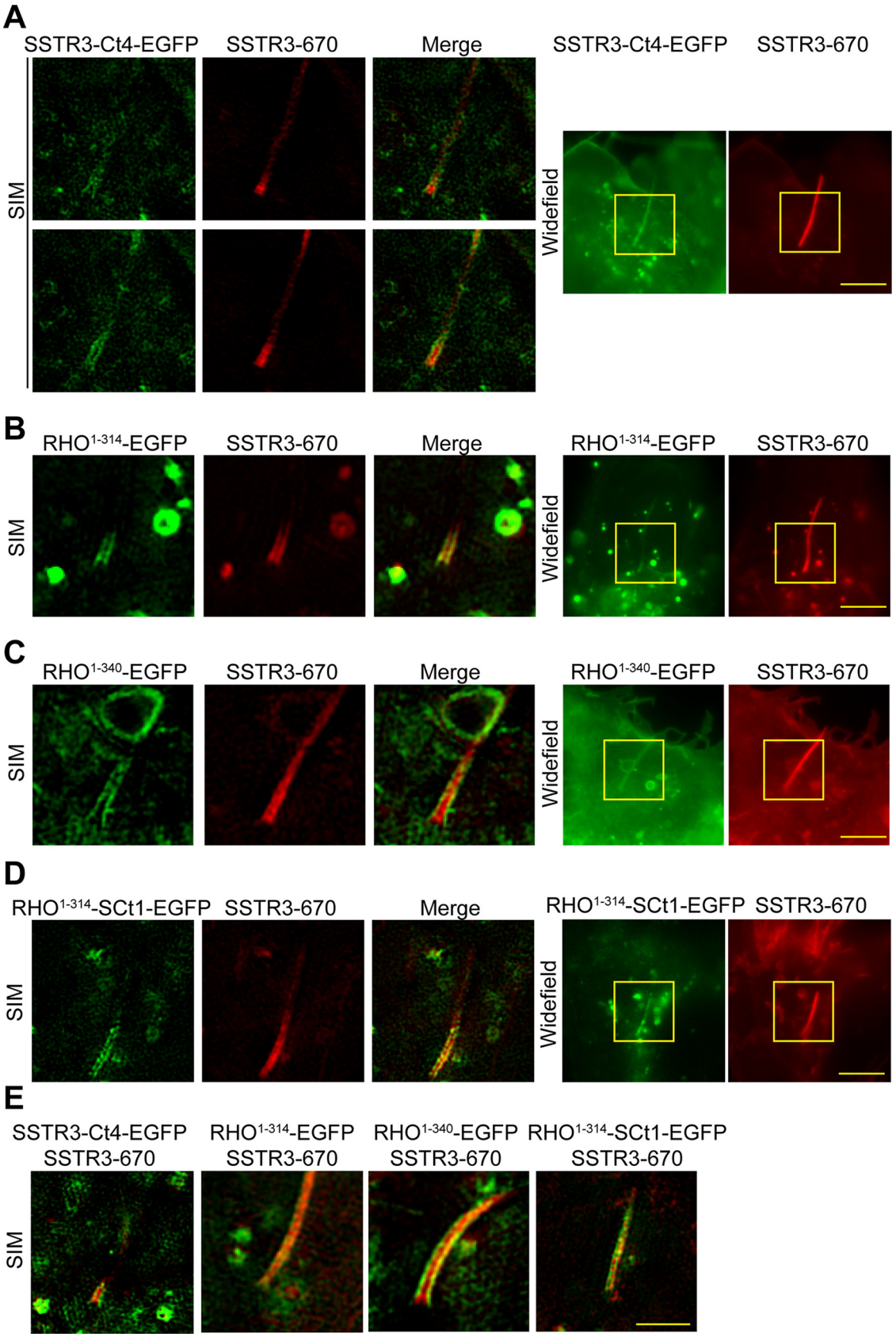

Figure 6. Analysis of the C terminus of SSTR3 in ciliary localization, using SIM and wide-field imaging of live hTERT-RPE1 cells. ***A***, Two rows of SIM images, with each row showing different Z planes from the same cell. SSTR3-Ct4-EGFP, in which the C-terminal SSTR3 CLS has been disrupted, shows localization primarily to the ciliary pocket. (The SSTR3-Ct4-EGFP has an N terminal avitag that was not used for this experiment.) ***B***, Deletion of the C terminus of RHO (to generate RHO^{1-314}) promoted localization to the ciliary membrane versus the periciliary membrane. ***C***, RHO^{1-340} localized mostly to the periciliary membrane. ***D***, Addition of a 32-amino-acid CLS from SSTR3 (SCt1) to RHO^{1-314} resulted in localization mostly to the ciliary membrane; but as RHO^{1-314} had a similar localization, no effect of adding SCt1 was detectable. (RHO^{1-314}-EGFP, RHO^{1-340}-EGFP and $RHO1^{-314}$-SCt1-EGFP all have an N-terminal avitag that was not used for these

of SCt1 on RHO^{1-314}-EGFP. RHO^{1-314}-SCt1-EGFP localized in the same manner as RHO^{1-314}-EGFP, showing that the addition of SCt1 at least did not dislocalize the RHO^{1-314}-EGFP; it had no net effect (Fig. 6*D*,*E*). Both proteins (without or with SCt1) exhibited a significantly higher percentage of fluorescence in the ciliary membrane than RHO-EGFP-C8 (Fig. 5*C*).

These results suggest that all or part of the RHO C terminus, beyond residue 314, promotes localization to the periciliary membrane, rather than the ciliary membrane, of hTERT-RPE1 cells. To test whether the terminal 8 residues of RHO (which are repeated after the EGFP in RHO-EGFP-C8) were required for this localization, we investigated the localization of RHO^{1-340}-EGFP. We found that RHO^{1-340}-EGFP was primarily localized to the ciliary pocket, similar to RHO-EGFP-C8 (Figs. 5*C*, 6*C*,*E*). Therefore, the region of RHO that promotes localization to the periciliary membrane, rather than the ciliary membrane, in hTERT-RPE1 cells lies within residues 315–340.

Ciliary versus apical plasma membrane localization effect of SSTR3 C terminus on RHO in hTERT-RPE1 cells

The above analysis in hTERT-RPE1 cells focused on the relative localization between the periciliary pocket membrane and the ciliary membrane, regardless of targeting from the apical plasma membrane to the periciliary or ciliary membranes. To test whether the C terminus of SSTR3 can promote RHO localization to the ciliary plasma membrane relative to the apical plasma membrane, we compared CPIRs of RHO-EGFP-C8, RHO^{1-314}-EGFP, and RHO^{1-314}-SCt1-EGFP. To determine the CPIR of RHO-EGFP-C8, we used examples from confocal microscopy in which the cilium extended beyond the edge of the cell in the plane of imaging (Fig. 4*B*), so that there could be no contribution to the ciliary membrane signal from the periciliary membrane. Figure 5*D* shows CPIR measurements from the three proteins. Like the comparison between the periciliary and ciliary membranes, they show that the truncation of RHO, to create RHO^{1-314}-EGFP, results in increased localization in the RPE1 cilium. In addition, however, the CPIR measurements show that addition of the C terminus of SSTR3 to RHO^{1-314}-EGFP to generate RHO^{1-314}-SCt1-EGFP resulted in enhanced ciliary localization. Thus, the C terminus of SSTR3 promotes the ciliary localization of truncated RHO from the apical plasma membrane of hTERT-RPE1 cells.

Localization of different CD8A-SSTR3Ct chimeras indicate different membrane domains of the hTERT-RPE1 pocket cilium

SIM images demonstrated that CD8A-EGFP localizes mainly to the periciliary membrane rather than to the cilium (Fig. 7*A*,*E*). The addition of a 32-amino-acid motif from the proximal C terminus of SSTR3 (Fig. 2*A*, Ct1) promoted ciliary localization of CD8A-EGFP (Fig. 7*B*,*E*), which we confirmed by measurements of the proportion of cilium plus pocket fluorescence that was in the ciliary membrane (Fig. 7*D*), further arguing that the SSTR3 CLS enables proteins to pass into the cilium from the periciliary membrane.

Interestingly, a CD8A chimera in which the QE motif from SSTR3 is absent (Fig. 3, Ct3) resulted in highly specific localization to the periciliary membrane, relative not just to the ciliary plasma membrane but also relative to the rest of the plasma membrane. SIM images indicate localization to the periciliary membrane rather than the cilium, and wide-field images indicate that this CD8A chimera is minimally localized to the plasma membrane, although it does appear to accumulate in intracellular structures (Fig. 7*C*,*D*). This distribution is consistent with the periciliary membrane as a distinct membrane domain.

To quantify this periciliary membrane localization, we determined the targeting effect of SCt3 on CD8A-EGFP in terms of a periciliary to plasma membrane fluorescence intensity ratio (PCPIR). We used wide-field imaging to measure fluorescence levels of both CD8A-EGFP and CD8A-EGFP-SCt3, emitting from the periciliary membrane (SIM imaging showed negligible contribution from the ciliary membrane in both cases.) and from the adjacent plasma membrane. CD8A-EGFP exhibited a relatively low PCPIR value of 0.20 ± 0.03 ($N = 5$). By contrast, CD8A-EGFP-SCt3 had a PCPIR value of 6.4 ± 1.5 ($N = 8$), indicating that the SCt3 tag results in an ~30-fold increase in enrichment in the periciliary membrane versus the plasma membrane. This enrichment of CD8A-EGFP-SCt3 argues that the periciliary membrane is a distinct compartment for which SCt3 can provide a localization motif. It is consistent with the notion that the periciliary membrane has a specific function (such as a docking site en route to the cilium).

Requirement of TULP3 for the ciliary localization effect of the SSTR3 C terminus

We sought to gain molecular insight into how the SSTR3 C-terminal CLS localizes proteins to the cilium. Ciliary localization of SSTR3 has been shown to require TULP3, which is proposed to ferry numerous RHO family GPCRs into the cilium (Mukhopadhyay et al., 2010, 2013; Badgandi et al., 2017), but how SSTR3 interacts with TULP3 has not been determined. Our findings suggest that the C-terminal CLS of SSTR3 might be important in TULP3 interaction.

To test this suggestion, we generated a knockout of TULP3 in hTERT-RPE1 cells using a CRISPR sgRNA previously shown to be viable in that cell type (Han et al., 2019). We obtained a pure population of cells with a two-base pair deletion, which was expected to result in an early stop because of a frameshift mutation. Western blot analysis confirmed loss of TULP3 protein in the knockout (Fig. 8*A*). The resulting TULP3-null hTERT-RPE1 cells were then transfected to express chimeric proteins whose ciliary localization are enhanced by the inclusion of the 32-amino-acid CLS from the SSTR3 C terminus. The location of the cilium was identified after fixation using acetylated α-tubulin labeling as cilium GPCR markers were not expected to localize well in cells lacking TULP3.

We studied the ciliary localization of the CD8A-EGFP-SCt1 chimera (Fig. 3*C*) and found that the ciliary localization was reduced by ~85% in TULP3 null cells compared with WT cells (Fig. 8*C*). Similarly, the Rho^{1-314}-SCt1-EGFP chimera (Figs. 5*C*, 6*B*) also exhibits a greatly reduced CPIR in TULP3-null cells (Fig. 8*B*,*C*). Expression of an mKate2-TULP3 rescue construct enhanced CPIR values of Rho^{1-314}-SCt1-EGFP in TULP3-null cells, indicating that the reduced localization of the SCt1-containing chimeras was specifically because of the loss of TULP3 (Fig. 8*D*). Therefore, the C-terminal CLS of SSTR3 requires TULP3 to effect ciliary localization.

←

experiments.) Scale bars, 5 μm. ***E***, Additional merged examples of images shown in ***A–D***. Scale bars, 2 μm. Yellow squares on wide-field images correspond to the regions shown in the SIM panels.

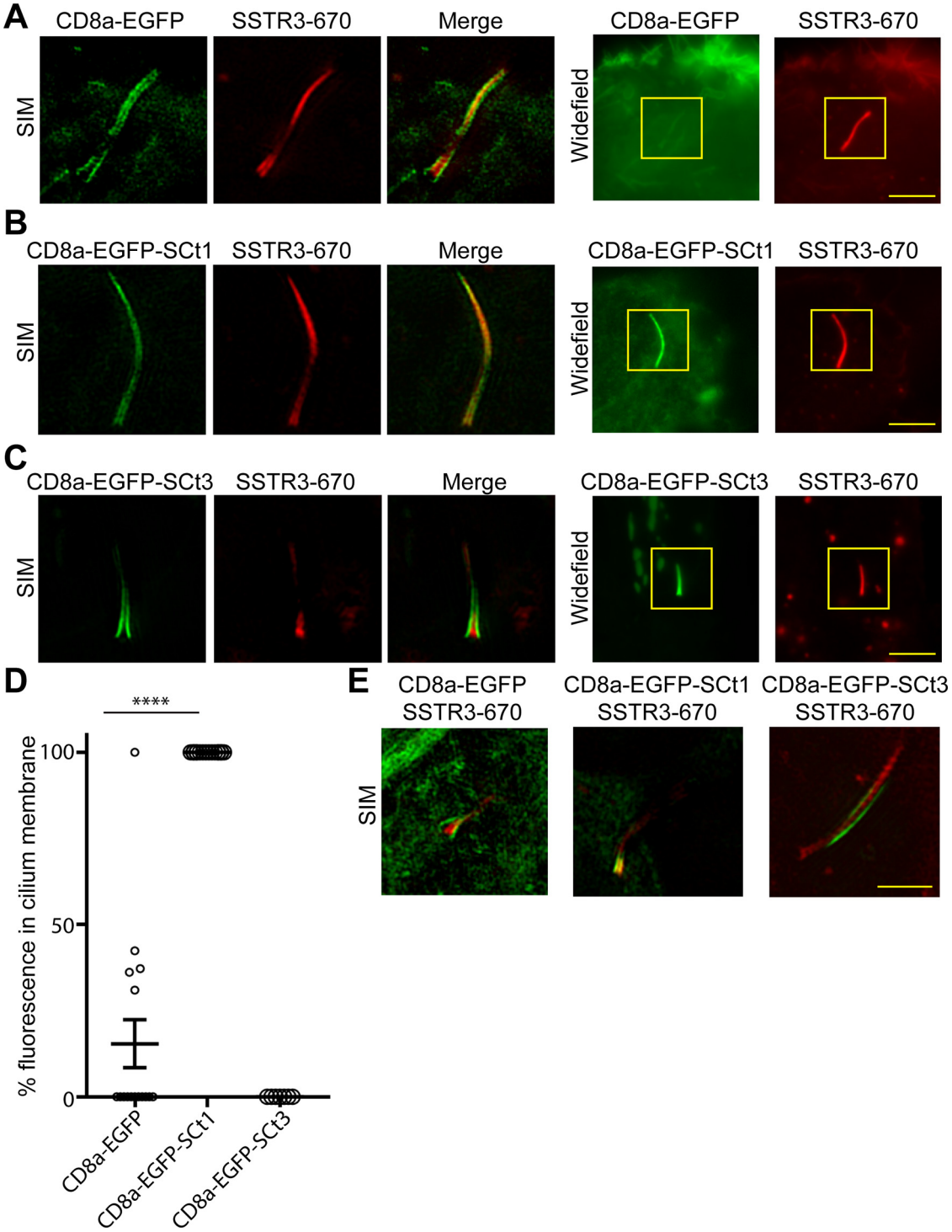

Figure 7. Ciliary localization of CD8A-EGFP chimeras, containing parts of the SSTR3 C terminus, using SIM and wide-field imaging of live hTERT-RPE1 cells. ***A***, Localization of CD8A-EGFP to the ciliary pocket. Wide-field images indicate substantial localization also to the plasma membrane. ***B***, Addition of SCt1 to CD8A-EGFP results in ciliary localization. ***C***, A truncated SSTR3 CLS results in more specific localization to the periciliary membrane (pocket). Wide-field images indicate localization in some intracellular structures but much less associated with the rest of the apical plasma membrane (cf. ***A***). SIM indicates that the localization in the proximity of the cilium is in the periciliary membrane (pocket). Scale bars, 5 μm. ***D***, Comparison of the percentage of fluorescence in the ciliary membrane for CD8A-EGFP, CD8A-EGFP-SCt1 and CD8A-EGFP-SCt3 from SIM experiments in live hTERT-RPE1 cells; $n = 7–16$. ****$p < 0.0001$. Error bars indicate means ± SEM. ***E***, Additional examples of images shown in ***A–C***. Scale bars, 2 μm. Yellow squares correspond to the regions shown in the SIM panels.

Localization to the cilium (i.e., outer segment) of the mouse rod photoreceptor *in vivo*

The C terminus of RHO has been found to be important in localization to the photoreceptor OS. C-terminal mutations, in particular the RHO Q344ter mutation, result in RHO mislocalization in mouse photoreceptors (Sung et al., 1994; Li et al., 1996; Concepcion and Chen, 2010). The same phenotype was observed in frog photoreceptors (Tam et al., 2000; Lodowski et al., 2013), however, in that system, it was observed that deletion of the entire C-terminal region of RHO resulted in normal

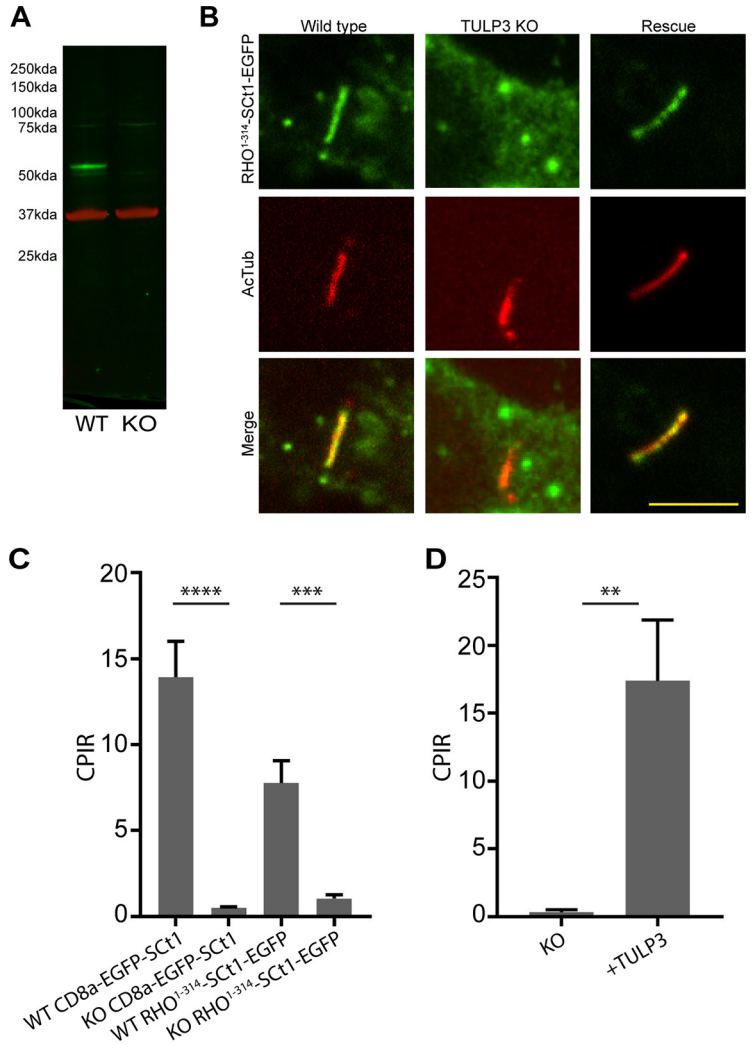

Figure 8. TULP3 mediates the localization of the C-terminal SSTR3 CLS to the cilium in hTERT-RPE1 cells. ***A***, Western blot, labeled with antibodies against TULP3 (green) and GAPDH (red), indicating knockout of TULP3 in the predicted null cells (KO). ***B***, Representative spinning disk confocal microscope images of fixed hTERT-RPE1 cells expressing Avi-RHO$^{1\text{-}314}$-SCt1-EGFP and stained for acetylated α-tubulin. Ciliary localization of Avi-RHO$^{1\text{-}314}$-SCt1-EGFP is reduced in the TULP3-null line. Scale bar, 5 µm. ***C***, Knockout of TULP3 resulted in significantly less ciliary localization for CD8A-EGFP-SCt1 and Avi-RHO$^{1\text{-}314}$-SCt1-EGFP, as determined by CPIR measurements. Wild-type RHO$^{1\text{-}314}$-SCt1-EGFP, $n = 28$ (3 experiments); TULP3 knockout RHO$^{1\text{-}314}$-SCt1-EGFP, n 15 (4 experiments); wild-type CD8A-EGFP-SCt1, $n = 28$ (3 experiments); TULP3 knockout CD8A-EGFP-SCt1, $n = 11$ (4 experiments); ****$p < 0.0001$, Kruskal–Wallis test with *post hoc* Dunn's multiple comparisons test; error bars are means ± SEM. ***D***, Cotransfection of Avi-RHO$^{1\text{-}314}$-SCt1-EGFP and mKate2-TULP3 resulted in rescue of the reduced CPIR observed in TULP3 knockout cells. TULP3 knockout, $n = 11$ (2 experiments); TULP3 knockout rescue, $n =$ 15 (2 experiments). **$p < 0.01$, Mann–Whitney *U* test. Error bars are means ± SEM.

localization of RHO, suggesting the presence of a mislocalization motif further upstream in the C-terminal region (Lodowski et al., 2013).

To define the C-terminal CLS of mouse RHO better, we extended our studies, using subretinal electroporation of WT mice with fluorescently tagged constructs, as in Figure 1*E* and Movie 1. For quantification, we divided the average fluorescence in the outer segment by the sum of the average fluorescence in outer and inner segments to obtain the proportion of fluorescence in the outer segment. Compared with RHO-EGFP, RHO$^{1\text{-}340}$-EGFP (lacking the last eight amino acids) showed a reduction in the proportion of fluorescence in the outer segment. Deletion of the entire C terminus of RHO (RHO$^{1\text{-}314}$-EGFP), however, resulted in a much larger decrease in OS localization (Fig. 9*A*,*B*). These results indicate that unlike the case in frogs (and in hTERT-RPE1 cells; Fig. 5*C*), amino acids 315–340 of RHO do not appear to contain a mislocalization motif in mouse photoreceptors and instead play a role in enrichment to the OS.

As we had found that SSTR3-EGFP also localized to rod outer segments (Fig. 1*E*), we tested whether the SSTR3 C-terminal CLS could function in photoreceptor cells, as we found in IMCD3 and hTERT-RPE1 cells. We addressed whether the C-terminal CLS of SSTR3 could replace the function of the RHO C-terminal CLS by expressing the RHO$^{1\text{-}314}$-SCt1 chimera in photoreceptors. We found that addition of the SSTR3 CLS resulted in significant enrichment relative to RHO$^{1\text{-}314}$-EGFP, although not as much as full-length RHO-EGFP or RHO$^{1\text{-}340}$-EGFP (Fig. 9*A*,*B*).

As a complementary approach, we tested chimeras of CD8a-EGFP to investigate the role of CLSs in localization to the outer segment. Consistent with our results using RHO-SSTR3 chimeras, CD8a-EGFP-SCt1 and especially CD8a-EGFP-RHOCt (containing the terminal 38 amino acids of RHO) enhanced localization of CD8a-EGFP to the outer segment (Fig. 9*C*,*D*).

Discussion

SSTR3 localized specifically to the ciliary membrane in IMCD3 and RPE1 cells, representing nonpocket and pocket cilia, respectively. By contrast, the ciliary localization of RHO in these cells was variable and, on average, weak, despite a high specificity for the photoreceptor cilium (OS), where it was extremely concentrated. The converse was not true: SSTR3 showed robust localization to the photoreceptor OS, indicating that the photoreceptor cilium is less selective than the simpler primary cilia. These findings also suggest that CLSs exert cell-type specific effects. To dissect these effects in more detail, we characterized a C-terminal CLS in SSTR3, which promoted ciliary localization of SSTR3 in IMCD3 and RPE1 cells. When added to CD8A or replacing the C terminus of RHO, the resulting chimeric protein localized to the cilia of these cells more specifically. This SSTR3 C-terminal CLS was also effective in increasing the photoreceptor OS localization of CD8A-EGFP or truncated RHO (RHO$^{1\text{-}314}$), although not to the same extent as the RHO C terminus. Our results increase our understanding of how GPCRs localize to cilia. They also demonstrate that although ciliary localization can be achieved in heterologous expression systems, the extent of localization differs according to specific CLSs, as well as the nature of the particular cilium.

Numerous studies have shown strong and specific localization of SSTR3 to the IMCD3 cilium (Berbari et al., 2008a; Hu et al., 2010; Ye et al., 2013). SSTR3 has also been localized to the RPE1 cilium (Mukhopadhyay et al., 2010; Tian et al., 2014; Madugula

and Lu, 2016), although the present study is the first to resolve that the localization is specifically to the ciliary plasma membrane and not the closely apposed periciliary membrane. The generation of high-quality SIM images of closely apposed biological structures is dependent on the signal-to-noise ratio of those structures. When signal-to-noise ratios are low, the SIM reconstruction process results in artifacts that can make it difficult to properly resolve and measure fluorescence intensities in closely apposed structures.

The last eight amino acids of RHO are heavily implicated in trafficking to photoreceptor outer segments (Li et al., 1996; Tam et al., 2000; Concepcion and Chen, 2010; Lodowski et al., 2013; Pearring et al., 2013). At the same time, sequences within $RHO^{322-336}$ act as a secondary inhibitory sequence in frog photoreceptors (Lodowski et al., 2013), driving RHO mislocalization in the absence of the VxPx motif. We found that in hTERT-RPE1 cells, RHO-EGFP-C8 and RHO^{1-340}-EGFP localized more to the ciliary pocket, whereas RHO^{1-314}-EGFP localized more to the ciliary membrane. This result suggests that the VxPx motif did not appear to strongly affect RHO localization in hTERT-RPE1 cells. The observation that the region from $RHO^{315-340}$ promoted mislocalization to the ciliary pocket is in accord with the results of Lodowski et al. (2013) and suggest an interaction in that region of the C terminus that inhibits ciliary localization in hTERT-RPE1 cells. Unlike the case in frog photoreceptors and hTERT-RPE1 cells, however, RHO^{1-314}-EGFP showed much less robust localization to the outer segment than RHO^{1-340}-EGFP, indicating that this region of RHO may act as either an inhibitory or positive signal for ciliary localization, depending on the cell type.

SSTR3 has been used as a model GPCR to investigate ciliary trafficking mechanisms, such as the role of the BBSome in ciliary retrieval (Ye et al., 2018) and ciliary entry (Berbari et al., 2008b; Jin et al., 2010), as well as the role of β-arrestin (Green et al., 2016) and Rab proteins (Tower-Gilchrist et al., 2011) in ciliary trafficking, and robust ciliary localization has been advantageous in studies of intraciliary protein movement (Ye et al., 2013; Lee et al., 2018). With regard to ciliary localization, studies had focused on the IC3 of SSTR3, which was found to contain an important CLS (Berbari et al., 2008a; Barbeito et al., 2021). The third intracellular loop of SSTR3 was also used to generate a chimeric RHO-i3SR3-EGFP protein to enhance ciliary enrichment of RHO *in vitro* and thereby study intraciliary trafficking of RHO using single-molecule tracking (Geneva et al., 2017; Lee et al., 2018). Replacement of the C terminus of RHO with the SSTR3 CLS resulted in a higher CPIR (Fig. 2*D–F*) than that observed for studies of RHO-i3SSTR3 (Geneva et al., 2017). In some cases, therefore, replacing RHO with RHO^{1-314}-SCt (RHO with the C terminus replaced by that of SSTR3) might be advantageous for in vitro studies of RHO because of the greater fidelity of localization to the ciliary plasma membrane.

During the course of our study, Barbeito et al. (2021) reported the presence of a C-terminal CLS in SSTR3 and HTR6, expressed

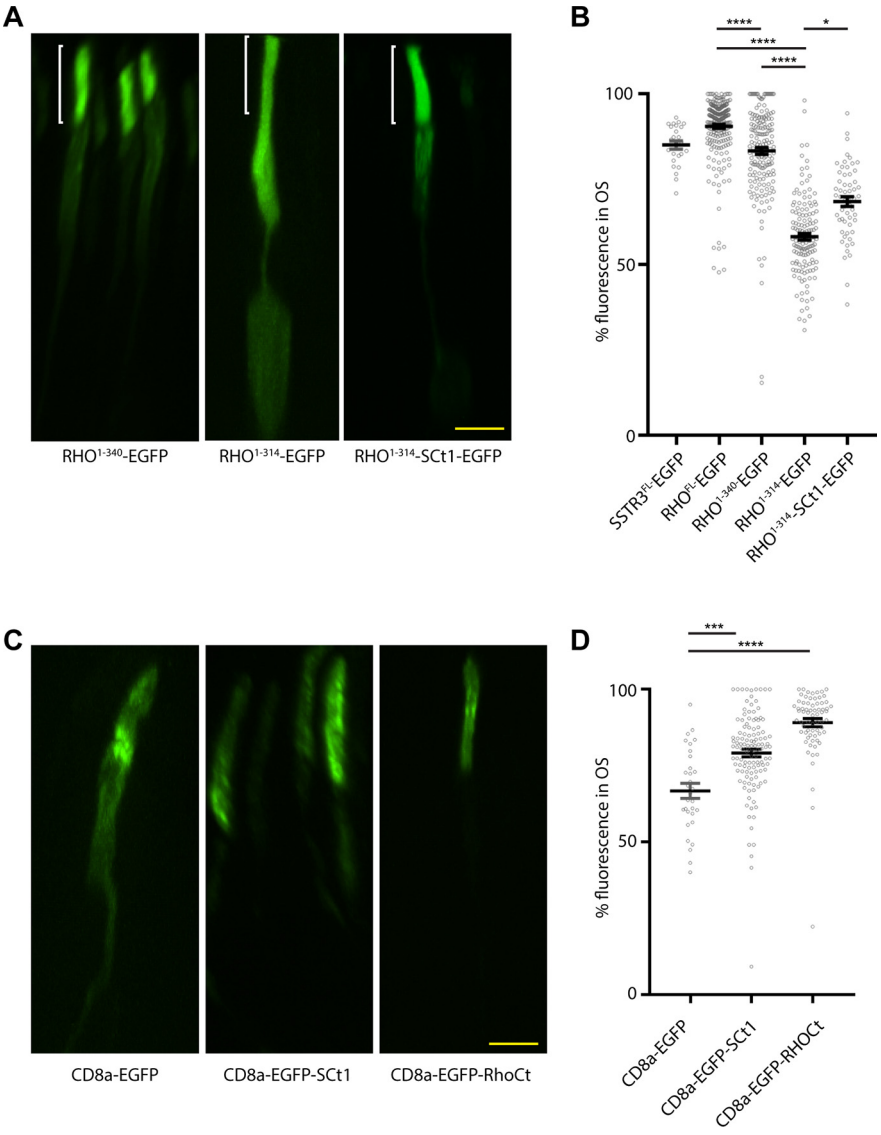

Figure 9. Comparison of GPCR localization in mouse photoreceptors. ***A***, Orthogonal view of a mouse photoreceptor electroporated with EGFP-tagged RHO lacking the C-terminal 8 amino acids (RHO^{1-340}), RHO missing the entire C terminus (RHO^{1-314}), and RHO with the C-terminal 34 amino acids replaced by SCt1 (RHO^{1-314}-SCt1). Localization to the outer segment layer was confirmed by colabelling with WGA-647 and by the observation of the inner segment and nucleus by faint EGFP labeling (OS is indicated by white bracket). Scale bar, 5 μm. ***B***, Average percentage of fluorescence in the outer segment relative to the sum of the outer and inner segments was obtained from profiles of photoreceptors electroporated with various GPCRs. $SSTR3^{FL}$-EGFP, $n = 25$ cells; RHO^{FL}-EGFP, $n = 241$ cells; RHO^{1-340}-EGFP, $n = 172$ cells; RHO^{1-314}-EGFP, $n = 144$ cells; RHO^{1-314}SCt1-EGFP, $n = 57$ cells. $^{*}p < 0.05$, $^{***}p < 0.001$, $^{****}p < 0.0001$, Kruskal–Wallis test with *post hoc* Dunn's multiple comparisons test. Error bars are means ± SEM. ***C***, Orthogonal views of a mouse photoreceptor electroporated with CD8a-EGFP, CD8a-EGFP appended with 32 amino acids including the C-terminal CLS of SSTR3 (CD8a-EGFP-SCt1) and CD8a-EGFP appended with 38 amino acids from the C terminus of RHO (CD8a-EGFP-RhoCt). Scale bar, 5 μm. ***D***, Average percentage of fluorescence in the outer segment from profiles of photoreceptors electroporated with CD8a-EGFP chimeras. CD8A-EGFP, $n = 31$ cells; CD8A-EGFP-SCt1, $n = 121$ cells; CD8A-EGFP-RHOCt, $n = 69$ cells. $^{***}p < 0.001$, $^{****}p < 0.0001$, Kruskal–Wallis test with *post hoc* Dunn's multiple comparisons test. Error bars are means ± SEM.

in IMCD3 cells. This work, which was focused mainly on HTR6, used some different approaches from ours to characterize the CLS, resulting in some different conclusions as well as some in common. A major difference is that this group concluded that the C-terminal CLS and the CLS in the third intracellular loop of SSTR3 were completely redundant. In our hands, the C-terminal CLS was essential for robust WT ciliary localization in IMCD3 cells, as well as in RPE1 cells. This difference may be because of our assessment, based on the extent of enrichment in individual cilia; in contrast Barbeito et al. determined the fraction of cilia exhibiting a detectable signal. Both studies used CD8A chimeras to help define that the C-terminal CLS is essential, although our analysis of CD8A chimeras refined the sufficient domain for ciliary localization to a 20-amino-acid sequence in the SSTR3 C terminus. In a candidate approach, Barbeito et al., concluded that the FK and LLRP amino acids are the most important components of the SSTR3 C-terminal CLS. In contrast, we performed an unbiased alanine scan, which indicated that the critical motif was the RPSRRI sequence.

The periciliary membrane of pocket cilia appears to be an active site of endocytosis (Molla-Herman et al., 2010) or vesicular docking (Papermaster et al., 1985; Deretic and Papermaster, 1991). Here, we found that an incomplete CLS could result in enrichment, specifically in the periciliary membrane of hTERT-RPE1 cells (and not throughout the plasma membrane). The CD8A-EGFP-SCt3 protein localized to the plasma membrane of IMCD3 cells, whereas in hTERT-RPE1 cells, it was localized specifically to the periciliary membrane, over both the ciliary membrane and the rest of the apical plasma membrane (Fig. 7). This indicates that the CD8A-EGFP-SCt3 protein was constrained to the periciliary membrane by binding to an associated structure, such as the described actin network (Molla-Herman et al., 2010), or that the periciliary membrane is physically separated from the rest of the cell, with a barrier between it and the rest of the plasma membrane, perhaps similar to that at the entry to the ciliary plasma membrane. Such a notion is consistent with observations of an accumulation of activated TGFβ near the base of the pocket cilium of mouse embryonic fibroblasts (Molla-Herman et al., 2010; Clement et al., 2013) and the observation that the flagellar collar of *Trypanosoma brucei*, which is homologous to the ciliary pocket, acts to restrict movement between the flagellar pocket and plasma membrane (Gerrits et al., 2002; Mussmann et al., 2003; Field and Carrington, 2009; Lacomble et al., 2009).

Previous studies had indicated that SSTR3 requires TULP3 for ciliary localization (Mukhopadhyay et al., 2010), although it has remained unclear how TULP3 mediates ciliary localization. The third intracellular loop of GPR161 and MCHR1 were sufficient to promote ciliary entry of CD8A chimeras in a TULP3-dependent fashion, but no such interaction was reported for SSTR3 (Badgandi et al., 2017). Our results indicate that the C terminus of SSTR3 is required for TULP3-mediated ciliary localization. Consistent with this observation, Barbeito et al. (2021) recently reported that a proximity labeling assay indicated association of TULP3 with the C terminus of SSTR3. The tubby protein family includes TUB and TULP1–4. These proteins feature a C-terminal domain that is highly conserved among them and interacts with ciliary localization sequences (Badgandi et al., 2017), and an N-terminal domain, which in the case of TULP3, TUBBY isoform b, and TULP2, interacts with IFT-A (Mukhopadhyay et al., 2010).

To briefly summarize, we have identified and characterized a novel CLS in SSTR3 and demonstrate that a given CLS may result in different localization patterns in different types of cilia, that is, cilia that emerge directly from the cell surface, cilia that are recessed in the cell and thus surrounded basally by a periciliary membrane (or pocket), and the elaborate phototransductive cilia of photoreceptor cells. Our results also further highlight the enigmatic nature of the $RHO^{315-340}$ C-terminal region, which promotes ciliary localization in mouse photoreceptors but promotes delocalization to the periciliary membrane in hTERT-RPE1 cells.

References

Badgandi HB, Hwang SH, Shimada IS, Loriot E, Mukhopadhyay S (2017) Tubby family proteins are adapters for ciliary trafficking of integral membrane proteins. J Cell Biol 216:743–760.

Barbeito P, Tachibana Y, Martin-Morales R, Moreno P, Mykytyn K, Kobayashi T, Garcia-Gonzalo FR (2021) HTR6 and SSTR3 ciliary targeting relies on both IC3 loops and C-terminal tails. Life Sci Alliance 4: e202000746.

Berbari NF, Johnson AD, Lewis JS, Askwith CC, Mykytyn K (2008a) Identification of ciliary localization sequences within the third intracellular loop of G protein-coupled receptors. Mol Biol Cell 19:1540–1547.

Berbari NF, Lewis JS, Bishop GA, Askwith CC, Mykytyn K (2008b) Bardet-Biedl syndrome proteins are required for the localization of G protein-coupled receptors to primary cilia. Proc Natl Acad Sci U S A 105:4242–4246.

Borman AD, Pearce LR, Mackay DS, Nagel-Wolfrum K, Davidson AE, Henderson R, Garg S, Waseem NH, Webster AR, Plagnol V, Wolfrum U, Farooqi IS, Moore AT (2014) A homozygous mutation in the TUB gene associated with retinal dystrophy and obesity. Hum Mutat 35:289–293.

Burgoyne T, Meschede IP, Burden JJ, Bailly M, Seabra MC, Futter CE (2015) Rod disc renewal occurs by evagination of the ciliary plasma membrane that makes cadherin-based contacts with the inner segment. Proc Natl Acad Sci U S A 112:15922–15927.

Chadha A, Volland S, Baliaouri NV, Tran E, Williams DS (2019) The route of the visual receptor, rhodopsin, along the cilium. J Cell Sci 132: jcs229526.

Clement CA, Ajbro KD, Koefoed K, Vestergaard ML, Veland IR, Henriques de Jesus MP, Pedersen LB, Benmerah A, Andersen CY, Larsen LA, Christensen ST (2013) TGF-β signaling is associated with endocytosis at the pocket region of the primary cilium. Cell Rep 3:1806–1814.

Concepcion F, Chen J (2010) Q344ter mutation causes mislocalization of rhodopsin molecules that are catalytically active: a mouse model of Q344ter-induced retinal degeneration. PLoS One 5:e10904.

Corbit KC, Aanstad P, Singla V, Norman AR, Stainier DY, Reiter JF (2005) Vertebrate smoothened functions at the primary cilium. Nature 437:1018–1021.

Deretic D, Papermaster DS (1991) Polarized sorting of rhodopsin on post-Golgi membranes in frog retinal photoreceptor cells. J Cell Biol 113:1281–1293.

Ding JD, Salinas RY, Arshavsky VY (2015) Discs of mammalian rod photoreceptors form through the membrane evagination mechanism. J Cell Biol 211:495–502.

Dryja TP, McGee TL, Hahn LB, Cowley GS, Olsson JE, Reichel E, Sandberg MA, Berson EL (1990) Mutations within the rhodopsin gene in patients with autosomal dominant retinitis pigmentosa. N Engl J Med 323:1302–1307.

Einstein EB, Patterson CA, Hon BJ, Regan KA, Reddi J, Melnikoff DE, Mateer MJ, Schulz S, Johnson BN, Tallent MK (2010) Somatostatin signaling in neuronal cilia is critical for object recognition memory. J Neurosci 30:4306–4314.

Field MC, Carrington M (2009) The trypanosome flagellar pocket. Nat Rev Microbiol 7:775–786.

Follit JA, Li L, Vucica Y, Pazour GJ (2010) The cytoplasmic tail of fibrocystin contains a ciliary targeting sequence. J Cell Biol 188:21–28.

Garcia G 3rd, Raleigh DR, Reiter JF (2018) How the ciliary membrane is organized inside-out to communicate outside-in. Curr Biol 28:R421–R434.

Garcia-Gonzalo FR, Corbit KC, Sirerol-Piquer MS, Ramaswami G, Otto EA, Noriega TR, Seol AD, Robinson JF, Bennett CL, Josifova DJ, Garcia-Verdugo JM, Katsanis N, Hildebrandt F, Reiter JF (2011) A transition zone complex regulates mammalian ciliogenesis and ciliary membrane composition. Nat Genet 43:776–784.

Geneva II, Tan HY, Calvert PD (2017) Untangling ciliary access and enrichment of two rhodopsin-like receptors using quantitative fluorescence microscopy reveals cell-specific sorting pathways. Mol Biol Cell 28:554–566.

Gerrits H, Mussmann R, Bitter W, Kieft R, Borst P (2002) The physiological significance of transferrin receptor variations in *Trypanosoma brucei*. Mol Biochem Parasitol 119:237–247.

Green JA, Schmid CL, Bley E, Monsma PC, Brown A, Bohn LM, Mykytyn K (2016) Recruitment of β-arrestin into neuronal cilia modulates somatostatin receptor subtype 3 ciliary localization. Mol Cell Biol 36:223–235.

Grossman GH, Watson RF, Pauer GJ, Bollinger K, Hagstrom SA (2011) Immunocytochemical evidence of Tulp1-dependent outer segment protein transport pathways in photoreceptor cells. Exp Eye Res 93:658–668.

Guadiana SM, Parker AK, Filho GF, Sequeira A, Semple-Rowland S, Shaw G, Mandel RJ, Foster TC, Kumar A, Sarkisian MR (2016) Type 3 adenylyl cyclase and somatostatin receptor 3 expression persists in aged rat neocortical and hippocampal neuronal cilia. Front Aging Neurosci 8:127.

Han S, Miyoshi K, Shikada S, Amano G, Wang Y, Yoshimura T, Katayama T (2019) TULP3 is required for localization of membrane-associated proteins ARL13B and INPP5E to primary cilia. Biochem Biophys Res Commun 509:227–234.

Howarth M, Takao K, Hayashi Y, Ting AY (2005) Targeting quantum dots to surface proteins in living cells with biotin ligase. Proc Natl Acad Sci U S A 102:7583–7588.

Hu Q, Milenkovic L, Jin H, Scott MP, Nachury MV, Spiliotis ET, Nelson WJ (2010) A septin diffusion barrier at the base of the primary cilium maintains ciliary membrane protein distribution. Science 329:436–439.

Jin H, White SR, Shida T, Schulz S, Aguiar M, Gygi SP, Bazan JF, Nachury MV (2010) The conserved Bardet-Biedl syndrome proteins assemble a coat that traffics membrane proteins to cilia. Cell 141:1208–1219.

Lacomble S, Vaughan S, Gadelha C, Morphew MK, Shaw MK, McIntosh JR, Gull K (2009) Three-dimensional cellular architecture of the flagellar pocket and associated cytoskeleton in trypanosomes revealed by electron microscope tomography. J Cell Sci 122:1081–1090.

Lee S, Tan HY, Geneva II, Kruglov A, Calvert PD (2018) Actin filaments partition primary cilia membranes into distinct fluid corrals. J Cell Biol 217:2831–2849.

Lehmann A, Kliewer A, Günther T, Nagel F, Schulz S (2016) identification of phosphorylation sites regulating sst3 somatostatin receptor trafficking. Mol Endocrinol 30:645–659.

Li T, Snyder WK, Olsson JE, Dryja TP (1996) Transgenic mice carrying the dominant rhodopsin mutation P347S: evidence for defective vectorial transport of rhodopsin to the outer segments. Proc Natl Acad Sci U S A 93:14176–14181.

Liu X, Udovichenko IP, Brown SD, Steel KP, Williams DS (1999) Myosin VIIa participates in opsin transport through the photoreceptor cilium. J Neurosci 19:6267–6274.

Liu X, Bulgakov OV, Darrow KN, Pawlyk B, Adamian M, Liberman MC, Li T (2007) Usherin is required for maintenance of retinal photoreceptors and normal development of cochlear hair cells. Proc Natl Acad Sci U S A 104:4413–4418.

Lodowski KH, Lee R, Ropelewski P, Nemet I, Tian G, Imanishi Y (2013) Signals governing the trafficking and mistrafficking of a ciliary GPCR, rhodopsin. J Neurosci 33:13621–13638.

Lopes VS, Jimeno D, Khanobdee K, Song X, Chen B, Nusinowitz S, Williams DS (2010) Dysfunction of heterotrimeric kinesin-2 in rod photoreceptor cells and the role of opsin mislocalization in rapid cell death. Mol Biol Cell 21:4076–4088.

Lu Q, Insinna C, Ott C, Stauffer J, Pintado PA, Rahajeng J, Baxa U, Walia V, Cuenca A, Hwang YS, Daar IO, Lopes S, Lippincott-Schwartz J, Jackson PK, Caplan S, Westlake CJ (2015) Early steps in primary cilium assembly require EHD1/EHD3-dependent ciliary vesicle formation. Nat Cell Biol 17:531.

Luo C, Wu M, Su X, Yu F, Brautigan DL, Chen J, Zhou J (2019) Protein phosphatase 1α interacts with a novel ciliary targeting sequence of polycystin-1 and regulates polycystin-1 trafficking. FASEB J 33:9945–9958.

Madugula V, Lu L (2016) A ternary complex comprising transportin1, Rab8 and the ciliary targeting signal directs proteins to ciliary membranes. J Cell Sci 129:3922–3934.

Maza NA, Schiesser WE, Calvert PD (2019) An intrinsic compartmentalization code for peripheral membrane proteins in photoreceptor neurons. J Cell Biol 218:3753–3772.

Molla-Herman A, Ghossoub R, Blisnick T, Meunier A, Serres C, Silbermann F, Emmerson C, Romeo K, Bourdoncle P, Schmitt A, Saunier S, Spassky N, Bastin P, Benmerah A (2010) The ciliary pocket: an endocytic membrane domain at the base of primary and motile cilia. J Cell Sci 123:1785–1795.

Mukhopadhyay S, Wen X, Chih B, Nelson CD, Lane WS, Scales SJ, Jackson PK (2010) TULP3 bridges the IFT-A complex and membrane phosphoinositides to promote trafficking of G protein-coupled receptors into primary cilia. Genes Dev 24:2180–2193.

Mukhopadhyay S, Wen X, Ratti N, Loktev A, Rangell L, Scales SJ, Jackson PK (2013) The ciliary G-protein-coupled receptor Gpr161 negatively regulates the Sonic hedgehog pathway via cAMP signaling. Cell 152:210–223.

Mussmann R, Janssen H, Calafat J, Engstler M, Ansorge I, Clayton C, Borst P (2003) The expression level determines the surface distribution of the transferrin receptor in *Trypanosoma brucei*. Mol Microbiol 47:23–35.

Nemet I, Ropelewski P, Imanishi Y (2015) Rhodopsin trafficking and mistrafficking: signals, molecular components, and mechanisms. Prog Mol Biol Transl Sci 132:39–71.

Nickell S, Park PS, Baumeister W, Palczewski K (2007) Three-dimensional architecture of murine rod outer segments determined by cryoelectron tomography. J Cell Biol 177:917–925.

Nishimura DY, Fath M, Mullins RF, Searby C, Andrews M, Davis R, Andorf JL, Mykytyn K, Swiderski RE, Yang B, Carmi R, Stone EM, Sheffield VC (2004) Bbs2-null mice have neurosensory deficits, a defect in social dominance, and retinopathy associated with mislocalization of rhodopsin. Proc Natl Acad Sci U S A 101:16588–16593.

Papermaster DS, Dreyer WJ (1974) Rhodopsin content in the outer segment membranes of bovine and frog retinal rods. Biochemistry 13:2438–2444.

Papermaster DS, Schneider BG, Besharse JC (1985) Vesicular transport of newly synthesized opsin from the Golgi apparatus toward the rod outer segment. Ultrastructural immunocytochemical and autoradiographic evidence in *Xenopus* retinas. Invest Ophthalmol Vis Sci 26:1386–1404.

Pearring JN, Salinas RY, Baker SA, Arshavsky VY (2013) Protein sorting, targeting and trafficking in photoreceptor cells. Prog Retin Eye Res 36:24–51.

Peters KR, Palade GE, Schneider BG, Papermaster DS (1983) Fine structure of a periciliary ridge complex of frog retinal rod cells revealed by ultrahigh resolution scanning electron microscopy. J Cell Biol 96:265–276.

Pihakaski-Maunsbach K, Nonaka S, Vorum H, Maunsbach AB (2010) Response of IMCD3 cells to hypertonic challenges as analyzed by electron microscopy. J Electron Microsc (Tokyo) 59:481–494.

Ran FA, Hsu PD, Wright J, Agarwala V, Scott DA, Zhang F (2013) Genome engineering using the CRISPR-Cas9 system. Nat Protoc 8:2281–2308.

Sjostrand FS (1953) The ultrastructure of the outer segments of rods and cones of the eye as revealed by the electron microscope. J Cell Comp Physiol 42:15–44.

Steinberg RH, Fisher SK, Anderson DH (1980) Disc morphogenesis in vertebrate photoreceptors. J Comp Neurol 190:501–508.

Sung CH, Makino C, Baylor D, Nathans J (1994) A rhodopsin gene mutation responsible for autosomal dominant retinitis pigmentosa results in a

protein that is defective in localization to the photoreceptor outer segment. J Neurosci 14:5818–5833.

Tam BM, Moritz OL, Hurd LB, Papermaster DS (2000) Identification of an outer segment targeting signal in the COOH terminus of rhodopsin using transgenic *Xenopus laevis*. J Cell Biol 151:1369–1380.

Tian G, Ropelewski P, Nemet I, Lee R, Lodowski KH, Imanishi Y (2014) An unconventional secretory pathway mediates the cilia targeting of peripherin/rds. J Neurosci 34:992–1006.

Tower-Gilchrist C, Lee E, Sztul E (2011) Endosomal trafficking of the G protein-coupled receptor somatostatin receptor 3. Biochem Biophys Res Commun 413:555–560.

Trivedi D, Colin E, Louie CM, Williams DS (2012) Live-cell imaging evidence for the ciliary transport of rod photoreceptor opsin by heterotrimeric kinesin-2. J Neurosci 32:10587–10593.

Volland S, Hughes LC, Kong C, Burgess BL, Linberg KA, Luna G, Zhou ZH, Fisher SK, Williams DS (2015) Three-dimensional organization of nascent rod outer segment disk membranes. Proc Natl Acad Sci U S A 112:14870–14875.

Wang J, Deretic D (2015) The Arf and Rab11 effector FIP3 acts synergistically with ASAP1 to direct Rabin8 in ciliary receptor targeting. J Cell Sci 128:1375–1385.

Wang J, Morita Y, Mazelova J, Deretic D (2012) The Arf GAP ASAP1 provides a platform to regulate Arf4- and Rab11-Rab8-mediated ciliary receptor targeting. EMBO J 31:4057–4071.

Williams DS (2002) Transport to the photoreceptor outer segment by myosin VIIa and kinesin II. Vision Res 42:455–462.

Wong SY, Reiter JF (2008) The primary cilium at the crossroads of mammalian hedgehog signaling. Curr Top Dev Biol 85:225–260.

Yang TT, Su J, Wang WJ, Craige B, Witman GB, Tsou MF, Liao JC (2015) Superresolution pattern recognition reveals the architectural map of the ciliary transition zone. Sci Rep 5:14096.

Ye F, Breslow DK, Koslover EF, Spakowitz AJ, Nelson WJ, Nachury MV (2013) Single molecule imaging reveals a major role for diffusion in the exploration of ciliary space by signaling receptors. Elife 2:e00654. e00654.

Ye F, Nager AR, Nachury MV (2018) BBSome trains remove activated GPCRs from cilia by enabling passage through the transition zone. J Cell Biol 217:1847–1868.